Effects of Thermomechanical Processing on Microstructure and Hardness Profiles in AA6061 Plates

A thesis submitted to the Faculty of Engineering and Built Environment of the University of Cape Town in fulfilment of the requirements for the degree of Master of Science in Applied Science

By

Innocent Hapazari

Centre for Materials Engineering

Department of Mechanical Engineering

University of Cape Town

December 2002

Abstract

Effects of rolling variables - strain (ε), strain rate (έ) and temperature (T) - on grain structure and hardness evolution in AA6061 plates were investigated by simulating the rolling process using plane strain compression (PSC). Particular emphasis was exerted on understanding the impact of the variables on the overall mean grain size and hardness, as well as how they influence the grain size and hardness profiles through the thickness of the rolled plates.

Prior to PSC investigations, the grain size and hardness profiles of the supplied material (transfer and finished plates) were determined using a Reichert MeF3A optical microscope and Vickers hardness tester. No significant grain size variations were observed through the thickness of transfer plate. On the contrary, finished plates exhibited grain size gradients, with grain size progressively decreasing from the surface to the centre of the plate thickness. Hardness measurements did not exhibit any through-thickness variations, in both transfer and finished plates tested in as-deformed state. However, heat-treated samples, from both the transfer and finished plates, showed slight through-thickness variations in hardness, which were attributed to residual stresses arising from quenching process.

A series of 1-pass and 2-pass plane strain compression (PSC) tests were performed on AA6061 samples over a matrix of the deformation variables (ε, έ and T). The respective variable ranges investigated were: temperature, from about 200°C to 370°C; strain, from 0.2 to 1.0; and strain rate, from $2s^{-1}$ to $10s^{-1}$. All PSC deformed samples were subsequently analysed for grain size and hardness. The results showed that grain size increases with increase in deformation temperature, while it decreases with increase in strain and strain rate. In heat-treated plates, hardness was found to be generally insensitive to any of the investigated variables – with measured values from all samples being practically similar.

A numerical finite element model (FEM) predicted that, at the rolling instant, the centre of the work-piece experiences the highest temperatures accompanied by lowest strains and lowest stain rates, relative to the rest of the body. The parameters change progressively towards plate surface, with the outermost (surface) element- layer experiencing the lowest temperatures, highest strains and highest strain rates. Selected FEM outputs were used as PSC inputs to simulate through-thickness rolling conditions. Subsequent microstructure analyses gave a finer grain structure on the surface relative to the centre of the plate. From the FEM and PSC simulations results, theoretically, a rolled plate would, therefore, always be expected to exhibit a finer grain structure on surface relative to its centre. In practice, however, situations where the grain size gradient trend is completely opposite to this prediction are common, as also observed in the commercial finished plates investigated here. This suggests, therefore, that the investigated variables cannot adequately account for grain size gradients observed in rolled plates. Optical microscopy was also used to characterize through-thickness particle distribution patterns; but no specific particle distribution trends or gradients were observed. Therefore, it was not possible to attribute the apparently inconsistent grain size patterns, in the commercial rolled plates, to particle distribution effects.

Acknowledgements

"If I have seen further, it is by standing on the shoulders of the giants" – Sir Isaac Newton

I would like to thank the following people who, in their own various ways, made the completion of this academic phase relatively easier.

- My supervisor, Associate Professor R. D. Knutsen, for his supervision and guidance.
- Mr Gareth Floweday, for his tutoring skills and the many lunch-hours spent in CERECAM laboratory while introducing me to ABAQUS and modelling.
- Mr G. Newins and Mr P. Jacobs, for their machining expertise, which always made my subsequent sample preparation exercises much more enjoyable.
- Dr J. Zimba for readily availing himself for constructive discussions and at times asking very probing questions pertaining this project work.
- Hulett Aluminium, South Africa, for funding this research project and for the provision of the experimental samples.
- The Centre for Materials Engineering (UCT) and the International Postgraduate Scholarship (UCT) for jointly funding my studies.
- SIRDC (Zimbabwe) for giving me the opportunity to further my studies and also for the financial support.
- All members of staff and students in the Centre for Materials Engineering for their friendliness and co-operation, which I enjoyed over the years.
- Finally, all members of my family for all the sacrifices they have made so far towards my well-being. Without them I wouldn't have come this far. Special tribute to my wife, Josphine, and daughter, Chido, for patiently enduring my absence when they needed me most.

Table of Contents

Chapter 1

1 INTRODUCTION

AA6061 is an aluminium alloy, which belongs to a broad category of aluminium alloys designated as 6XXX series. The 6XXX is a group of heat-treatable alloys containing magnesium (Mg) and silicon (Si) as the main alloying elements. Minor additions, in strictly controlled amounts, of transition elements, such as, zirconium (Zr), manganese (Mn), iron (Fe) and copper (Cu), to impact specific properties to the alloy, are not uncommon. These alloys, like all other heat-treatable aluminium alloy series, that is 2XXX and 7XXX, derive their optimum mechanical strength properties from formation of secondary phase precipitates, within the aluminium matrix. In particular, the main strengthening phase in 6XXX alloys is Mg_2Si; and as a result Mg and Si are usually present in wt% amounts designed to meet the stoichiometric requirements for the formation of specific quantities of the Mg_2Si-phase. These commercial heat treatable alloys are widely used in rolled products due to their good performance and relatively low cost. More recently, the alloy series has gained the interest of the aircraft and automotive industries, due to potential enormous weight savings relative to steel, which is the traditional workhorse. Consequently, microstructural changes and the subsequent properties resulting from the thermomechanical processing of these alloys have become subjects of commercial and academic interest.

Some through-thickness microstructural variations, in terms of textures as well as grain size and morphology, and the concomitant property gradients have already been reported in various hot rolled plates. These observations are in line with the known inhomogeneities that accompany the deformation processes. For instance, during rolling process, the strains, strain rates and temperatures are known to vary through the thickness of the material being worked. These variations in turn influence microstructure evolution kinetics and hence the ultimate product properties, such as mechanical strengths, surface roughening, creep and corrosion

resistance, etc. However, the response to any given thermomechanical process depends on the specific alloy. The current study is therefore aimed at obtaining a detailed quantitative and qualitative understanding of the microstructures and properties that evolve in AA6061 plates as a result of different hot finishing mill schedules. The processing schedule encompasses critical variables, such as number of passes, inter-pass time, strain rate ($\dot{\varepsilon}$), strain (ε) and temperature (T). These parameters are known to influence the final product attributes. It is envisaged that a systematic evaluation of the microstructural and property response to the three, arguably most crucial, thermomechanical variables - strain rate, strain and temperature – will provide critical insight into the process-microstructure-property relationship in this particular alloy. The outcome of this work can potentially yield valuable technological benefits by providing industry with a well-researched basis for easier formulation of optimum combination(s) of temperature, strain and strain rate to achieve required microstructure and property targets. It is also expected to provide an insight into the available operational window within which the rolling process could be conducted without compromising the quality of the final product.

1.1 Objectives

Succinctly, the objectives of this project were initially set as:

- To investigate the evolution of microstructure and material properties of AA6061 as functions of thermomechanical variables - T, ε and $\dot{\varepsilon}$. Special effort being exerted on trying to understand if any of these variables is/are responsible for the through-thickness grain size gradients that have been observed in some rolled plates.
- To develop a numerical finite element model (FEM) to calculate the through-thickness distributions of ε, $\dot{\varepsilon}$ and T experienced by the work-piece during deformation.

- To use the FEM results as inputs in PSC tests in order to simulate different elements (from surface to centre) through the plate thickness. Then compare the characteristics of through-thickness microstructures of commercial plates, supplied by Hulett Aluminium, to those of simulated materials.

1.2 Experimental Approach

To achieve the afore-stated research objectives the following experimental approach was adopted.

- The through-thickness grain size and hardness values of the supplied material (transfer bar and finished plates) were determined using a Reichert MeF3A optical microscope and an ESE WAY hardness tester.

- A series of 1-pass and 2-pass plane strain compression (PSC) tests were performed on AA6061 samples over a matrix of deformation variables (ε, $\dot{\varepsilon}$ and T) in order to characterise the grain structure and hardness behaviour as functions of these variables. The test matrix was carefully selected in order to simulate industrial rolling conditions, encountered in the hot finish mill.

- A mathematical FEM, whose purpose was to determine through-thickness temperature, strain and strain rate distributions encountered during rolling, was formulated and executed using commercial finite element code, ABAQUS/Explicit, Version 6.2.1.

- The ε, $\dot{\varepsilon}$ and T predicted by the FEM were subsequently used as inputs in PSC tests to simulate the transient conditions experienced by specific regimes (from surface to centre) through the thickness of the work-piece.

The simulated through-thickness grain size patterns obtained from the PSC samples were compared with the grain size patterns observed in the commercial plates, supplied by Hulett Aluminium.

Chapter 2

2 LITERATURE REVIEW

2.1 Material

The material of focus in this study is an aluminium alloy designated AA6061. This is a commercial heat treatable alloy, which belongs to a broader category known as the 6XXX series. The 6XXX series consists of those aluminium alloys containing some additions of magnesium (Mg) and silicon (Si) as major alloying elements. The elements, Mg and Si, are crucial for the formation of Mg_2Si precipitate when the material is subsequently subjected to solution heat treatment and ageing conditions[1-4]. The two elements are added in balanced proportions to nominally combine as Mg_2Si. Excess Si may, however, be added to the alloy for increased strength, but to the detriment of corrosion resistance. Surplus Si enhances the alloy sensitivity to the ageing process by both refining the size of Mg_2Si particles and precipitating as Si[3]. In the 6XXX series the Mg content ranges from 0.6% to 1.2% with Si ranging from 0.35% to 1.3%[1]. Moreover, for AA6061, in particular, stipulated alloy element composition ranges are: (1) magnesium: 0.8 to 1.2 wt.% and (2) silicon: 0.4 to 0.8 wt.%[2,3,5]. The elements, Si and Mg, should be present in proportions such that the sum of their percentage weights is at least 1.5 wt.%. Deliberate additions of minor alloying elements such as copper (Cu), iron (Fe), manganese (Mn), chromium (Cr), and zirconium (Zr) are common. The trace elements are added in carefully controlled quantities dictated by the special properties required of the alloy[2,3].

2.1.1 AA6061 Chemistry

Typical chemical composition of AA6061 is given in Table 2-1.

Element	Mg	Si	Fe	Cu	Mn	Cr	Zn	Ti
Lower Limit wt%	0.8	0.4	-	0.15	-	0.35	-	-
Upper Limit wt%	1.2	0.8	0.7	0.4	0.15	0.05	0.25	0.25

Table 2-1. Typical Chemical Composition Limits of AA6061[2].

2.1.2 Effects of additional (trace) elements

Transition elements, such as Mn, Cr and Zr are generally added to control grain growth during thermomechanical processing. These metals tend to readily combine with Al to form intermetallic phases with very little or no solubility in the Al matrix. Due to their low diffusivity in Al, the alloying additions form very minute precipitates, usually less than 1μm in size, either during solidification or ingot preheating. This fine distribution of precipitates (or dispersoids) delays or even prevents static recrystallisation during processing. Moreover, the dispersoids are amenable to mechanical-fibering during processing; that is, they are strung out in the rolling direction, and in this way they aid in the retention of the elongated or "pancake"-shaped grains that develop during rolling. Also, the dispersoids possess larger mean free path in the rolling direction than in the perpendicular direction, thus recrystallised grains grow faster in the working direction[4]. Such elongated grains impart anisotropic behaviour in the material. Other components, such as Cu, tend to increase the strength of the alloy[2,3,6]. The 6XXX, Al-Mg-Si, alloys derive their optimum strengths from the presence of finely dispersed Mg_2Si precipitates. The alloy chemistry has immense influence on the material's response to post thermomechanical heat treatments and resultant properties. It is, therefore, imperative to get the alloy composition right if specific material attributes are to be achieved. The following are a few observations, by Zhuang et al[7], affirming the important interaction between composition of alloy and subsequent properties:-

- A relatively high Si/Mg ratio gives a good combination of mechanical properties.
- Mn concentrations should be strictly moderate – higher concentrations lead to poor ductility as well as poor formability, while lower concentrations may be insufficient for grain refinement, which is achieved by retarding grain growth of the recrystallised structure during solution heat treatment.

- Cr and Zr also retard grain growth during recrystallisation. Their grain refinement effectiveness also depends on their volume fractions and size of particles formed during the processes that precede solution heat treatment. The order of grain refinement effectiveness for the three elements, ideally, should be Zr > Cr > Mn, provided equal concentrations are applied and all additives are consumed to form dispersoid particles.

- The Mn/Fe ratio has also been observed to play an important role in controlling the degree of recrystallisation in the 6XXX alloys. Coarse constituent particles, such as AlFeMnSi, encourage formation of deformation zones around them. This has the effect of increasing or triggering particle stimulated nucleation (PSN) processes and thus reduces the recrystallisation resistance of the alloy for a given deformation. On the other hand, fine dispersoids of alumina formed during homogenisation increase the recrystallisation resistance of the alloy[8].

2.1.3 Microstructure and Mechanical Properties

Several researchers[6-9] have established that the principal microstructural features that control the mechanical properties of aluminium alloys are coarse intermetallic compounds, submicron dispersoids (0.05 to 0.5 μm), and fine precipitates (< 0.01 μm) produced by age hardening. In addition, grain size and shape, and dislocation

substructure also exert a significant influence on the mechanical properties. The way in which these aspects impact on the properties is further explained below:

- Coarse intermetallic compounds (usually in the size range 0.5 to 10 μm) form mainly during ingot solidification and they often contain iron and silicon impurity elements. They include virtually insoluble compounds $(Mn,Fe)Al_6$, $FeAl_3$, α-Al(Fe,Mn)Si, Al_7Cr_2Fe and the more soluble compounds, such as $CuAl_2$, Mg_2Si, and Al_2CuMg.
- The smaller, submicron compounds or dispersoids (0.05 to 0.5 μm) are intermetallic compounds usually containing transition metals chromium, manganese, or zirconium. Examples are $Al_{12}Mg_2Cr$ and $ZrAl_3$. The dispersoids serve primarily to retard recrystallisation and grain growth during processing and heat treatment of the respective alloys. They may also influence certain mechanical properties through their effects on both the material's subsequent response to ageing treatments and on dislocation microstructures formed during plastic deformation.
- Fine precipitates form during age hardening. They promote strengthening in alloys that respond to such treatments. The degree of strengthening depends primarily on the alloy system; for example, it increases in the order Al-Mg-Si, Al-Cu-(Mg) and Al-Zn-Mg-(Cu) when considering the common commercial alloys that respond to age hardening.
- Grain size and shape. Most wrought products do not undergo bulk recrystallisation during processing and subsequent heat treatments, so the elongated grain structure is retained. Three principal directions are generally recognised: longitudinal, long transverse and short transverse.

2.1.4 Strengthening Mechanisms in Aluminium Alloys

There is an increase in the recognition that the final use of a material should dictate the design and processing for the material. Therefore, a good understanding of the

strengthening mechanisms has become one of the crucial aspects needed to optimise process-structure-property relationships[10]. The following are some of the well-known strengthening mechanisms encountered in aluminium alloys.

a) Grain size effects:

According to Hall[11], aluminium and its alloys exhibit strengthening due to grain refinement governed by the well-known Hall-Petch relationship; Equation 2-1.

$$\sigma_F = \sigma_1 + kd^{-1/2}$$

Equation 2-1

Where: σ_F is the flow stress, σ_1 is a frictional stress, d is the average grain diameter, and k is a constant that characterises the difficulty of transmitting slip across the grain boundary for a given alloy system.

However, some work, for instance, Carreker and Hibbard[12], and Philips[13], have indicated that grain-size strengthening is not very strong in aluminium alloys. They attributed this to very small k-values, which they say are about five times less than in ferrous alloys. They, however, concurred that grain size effects become significantly influential at very fine grain sizes, in the range of $\leq 1\mu m$.

b) Solid-solution strengthening:

By applying Fleischer's approach[10,14], originally developed for copper alloys, strengthening from solute atoms arises from either, atomic size differences between the solute and the solvent atoms, or from differences in elastic modulus. Research by Noble et al[10,15], however, indicated that the size effect is the dominant source of solute strengthening in aluminium. The large solute effects in systems such as Al-Cu even make the analysis of the strengthening due to other factors, such as precipitate-hardening, very difficulty to analyse without ambiguity. Solutes are also known to introduce other effects, such as dynamic ageing with its concomitant serrated flow, in such aluminium alloys as Al-Mg[10].

b) Precipitate-hardening:

Second-phase particles, formed during solidification, mechanical processing and/or post-processing heat-treatment cycles, are known to give some aluminium alloys, particularly heat-treatable alloys, their optimum strengths. Heat-treatable, 2XXX (Al-Cu), 6XXX (Al-Mg-Si), and 7XXX (Al-Zr-Mg), alloys are strongly strengthened by precipitate hardening as well as solid solution hardening[10].

2.2 Thermomechanical Processing of Aluminium Alloys

Functional components from aluminium alloys are often produced via a thermomechanical processing route. This process involves the deformation of the cast slab (ingot) at specific temperatures, strains and strain rates, using processes such as rolling, extrusion and drawing[16,17]. These deformation processes usually result in the multiplication of defects, such as dislocations and interfaces, which in turn increase the free energy of the material. The deformed material is, thus, thermodynamically unstable. The thermomechanical processes and/or the post-deformation treatments on the material are usually tailored to restore the material to a more energetically stable state as well as optimise the material subsequent properties[16]. Of particular interest in this study is deformation by rolling.

The rolling deformation is usually preceded by a homogenisation stage. Homogenisation is a structure modification high temperature heat treatment process. For AA6061, typically, homogenisation is achieved by heating the ingots in a furnace at a nominal temperature of 525°C for at least 4 hours[18]. The applicable conditions are alloy-specific, however, the aim in almost all cases, is to eliminate solute concentration gradients (segregation) in the as-cast matrix. The process takes back into solid solution some of the elements precipitated at the casting stage and/or trigger diffusion mechanisms to allow a more even re-distribution of precipitates, which tend to segregate at the grain boundaries during

the casting processes. Furthermore, the solutes may re-precipitate in forms that optimise the subsequent behaviour of the material during further processing[18]. After homogenisation the material can then be rolled.

Rolling is a continuous deformation process designed to produce metallic sheets or plate. Rolling can be classified according to the rolls in the mill stand or according to the arrangements of the stand in sequence. But, more importantly, the rolling process is also usually classified as ***hot rolling*** or ***cold rolling***, depending on the temperature at which the deformation occurs. Rolling parameters, such as strain, strain rate, inter-pass time and temperature are critical. These parameters strongly influence the amount of stored energy in the deformed material[17,19], and consequently the process of recovery and recrystallisation.

2.2.1 Cold Rolling

When a material is rolled at a temperature below 0.6 of its melting point, the process is classified as cold rolling[17,20]. During cold rolling, the movement and annihilation of dislocations is very limited, this results in high dislocation density and hence high amount of deformation stored energy in the material. The lack of significant dynamic softening mechanisms, as in hot rolling, means higher deformation loads required. However, cold rolling has significant application, mostly in finishing mills, because it allows good gauge tolerances and gives bright clean surface finishes. Cold rolled materials generally exhibit high hardness (or strength), low toughness, low ductility, elongated deformed grain structure and anisotropy in mechanical properties.

2.2.2 Hot Rolling

When the material is deformed at temperatures above 0.6 of its absolute melting temperature the process is classified as hot rolling. One of the major advantages

of hot rolling is that it enables very heavy reductions per pass to be effected without applying excessive forces on the rollers and the work piece. It also improves the properties of the cast metal by breaking up the cast structure and refining the grain size, giving better homogeneity as well as greater strength and toughness[11,20]. Hot rolling is usually accompanied by restoration processes namely recovery and/or recrystallisation. When recovery or recrystallisation occurs concurrently with deformation, it is referred to as dynamic recovery or dynamic recrystallisation, respectively. However, whether a material undergoes one of the restoration processes or both during the deforming process depends on the material properties, especially the stacking fault energy (SFE). Materials of high stacking fault energy, such as aluminium, tend to undergo recovery much easier than materials with low stacking energy. The dynamic recovery phenomenon usually results in the attainment of a steady state condition in the deforming material, which is when the rate of dislocation generation is equivalent to the rate of dislocation annihilation by the recovery process. Very low or lack of recovery, in the low stacking fault energy materials, results in dislocation build-up which then acts as the driving force for the recrystallisation process. Thus, dynamic recrystallisation is more favourable in materials of low stacking fault energy[16,17,20]. In the case of dynamic recrystallisation, all the stored energy in the material is used up and new dislocation-free grains are formed; as such, any subsequent annealing treatments may result in grain growth.

Overall, plastic deformation leads to an increase in the free energy of a material as a result of increase in the structural defect density. The return to a more thermodynamically stable state is achieved by annealing out of those defects. The two main stages in the annealing process are recovery and recrystallisation[20-23].

2.2.2.1 Recovery

Recovery is the partial restoration of the original (undeformed) material properties by reduction of dislocation line energy stored during deformation. The reduction in

stored energy is due to re-arrangement of dislocations into low energy cell structures consisting of low angle boundaries, generally known as *subgrains*, whose interiors are relatively free of dislocations[20,22,23]. Figure 2-1 illustrates the formation of subgrains during the recovery process.

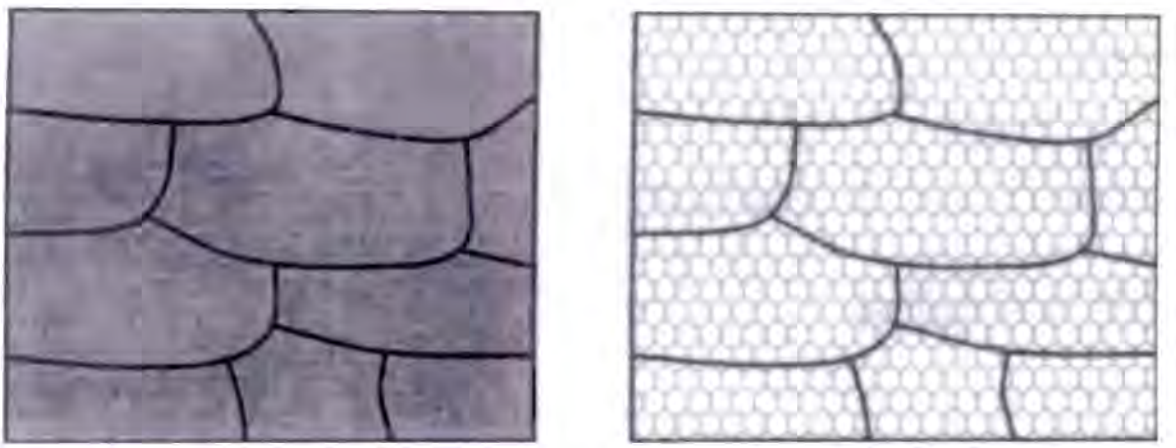

Figure 2-1. Stages of recovery: subgrain development through annihilation and rearrangement of dislocation (after Humphreys and Hatherly[20]).

Formation of subgrain structures could be depicted as a meta-stable state since a significant amount of stored energy of deformation is still available. As the recovery process proceeds, subgrains change shape through the migration of their boundaries. Boundary migration is caused by applied stress and/or subgrain growth. The subgrain boundary motion under stress generally accounts for dynamic recovery. On the other hand, subgrain growth is a post-deformation process, and hence it is responsible for static recovery. Subgrain growth results in reduction in the total area of low angle boundaries in a material, which in turn further reduces the stored energy of the material. This subgrain growth is a crucial aspect of thermomechanical processing because it determines the eventual softening mode of the deformed material. Full-scale (extensive) subgrain growth leads to softening entirely by extended recovery. The resultant extended recovered grains are typically elongated and of similar size scale as the initially deformed grains. In situations where only a few subgrains preferentially grow at the expense of other subgrains, then the subgrains that successfully grow will form

recrystallisation nuclei that grow to produce smaller, equi-axed grains. The major softening process in this case becomes recrystallisation[20,23].

2.2.2.2 Recrystallisation

Recrystallisation is the formation of new strain-free grains at the expense of the deformed or recovered microstructure. It is a softening process, in which the restoration of properties is complete. The recrystallised microstructure is usually characterised by equi-axed grain morphology. The driving force for recrystallisation is the availability of some excess dislocations (or stored energy) after the recovery process[20,23]. The basic stages of the recrystallisation are illustrated in Figure 2-2. The process is made up of two consecutive regimes, namely: nucleation and growth. Nucleation corresponds to the first appearance of new grains in small volumes at specific preferred sites, usually in regions of relatively higher lattice distortion, namely: the existing grain boundaries, deformation bands, inclusions, and other defects[23]. It is not a homogeneous process since it preferentially occurs at deformation heterogeneities. The nucleation process is usually quantified by the number of nuclei per unit volume of deformed structure; and it determines both the size and orientation of the subsequent grains. Growth is the phase in which newly formed grains expand and annihilate the deformed and/or recovered structure resulting in entirely new grain structure of lower dislocation density. Factors such as deformation temperature and strain, which influence amount of dislocations and the subsequent stored energy, have a significant effect on grain growth. The nucleation and growth processes do not necessarily occur separately and sequentially. In fact, they occur randomly and simultaneously; for example, occurrence of nucleation in one part of the microstructure could be accompanied by the grain growth in a different part of the same microstructure[20].

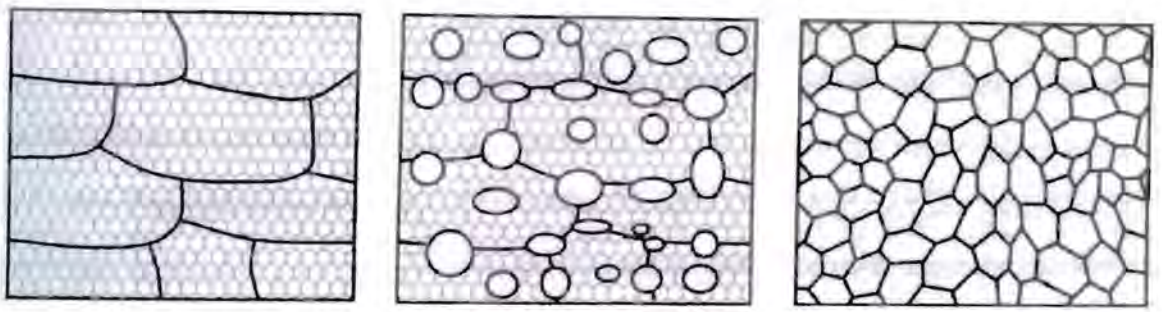

Figure 2-2. Stages of recrystallisation (after Humphreys and Hatherly[20]). Nucleation occurring in region of high misorientation; the newly forming grains impinge upon one another, after which grain growth will occur.

In addition to thermomechanical variables, material composition also plays an influential role in determining the restoration processes and hence ultimate microstructure and properties of the processed material. For instance, the presence of solid solute or precipitate particles in the material affects the kinetics of subgrain growth because the particles exert a pinning drag on the migrating subgrain boundaries. The drag is related to the size of particles by the Equation 2-2[20]: The effect is also known as the *Zener-pinning*, after Zener who first discovered the phenomenon.

$$P_z = (3F_v\gamma) / 2r$$

Equation 2-2

Where: P_z is the pinning pressure, F_v is the volume fraction of the particles, γ is the boundary energy and r is the radius of the particles.

A growing subgrain will have its effective driving force reduced as some of it is used to overcome the pinning pressure. This implies that in particular situations the subgrain network may be stabilised by the particles, forcing the material to remain recovered after post-deformation heat treatments (or annealing). This results in a microstructure closely similar to the deformed microstructure. The effectiveness of precipitating particles depends on their size and spacing. Closely

spaced particles exert a stronger pinning effect on the migrating high angle grain boundaries. On the other hand, coarsening of particles tends to reduce the pinning pressure and a stabilised subgrain network would eventually disintegrate.

2.2.3 Microstructural Evolution During Hot Rolling

Hot rolling is usually applied in a series of passes, which are separated by interpass times, which usually range from a few seconds to a couple of minutes. Industrial multi-pass rolling of aluminium alloys takes place at temperatures of between about 300°C and 500°C and strain rates ranging from about $0.1s^{-1}$ to $50s^{-1}$ [23]. The microstructural development that takes place in the material during rolling is a result of complex interaction between thermal, mechanical and metallurgical phenomena. Since properties of the final product are dependent on the developed microstructure, it is imperative to predict the microstructural evolution in order to anticipate the properties of the final product. At hot rolling temperatures, thermally activated deformation and restoration processes occur, and the microstructure evolution heavily depends on the deformation temperature, strain and strain rate. Several researchers[26,27,28], have been able to quantify deformation and annealing behaviour as a function of these variable parameters. The Zener-Hollomon parameter (Z) is often used to incorporate the deformation temperature and strain rate into a single variable, applying the relationship given in Equation 2-3. Z is also known as the temperature compensated strain rate and is used to cover a range of thermomechanical variables by assuming that the temperature of deformation can be compensated by changes in strain rate and vice-versa.

$$Z = \dot{\varepsilon} \exp (Q/RT)$$

Equation 2-3

Where: $\dot{\varepsilon}$ is the strain rate, Q is the activation energy of deformation for a given material, R is the gas constant and T is the absolute deformation temperature.

During rolling, the work-piece experiences some inhomogeneities in the distribution of the deformation variables through its thickness. This tends to result in differentials in stored energy through the material cross-section. The differences in the stored energy result in microstructure evolving differently through the thickness of the plate, thus resulting in variations in mechanical properties. The study of effects of thermomechanical variables on microstructure and mechanical properties is a subject that has generated intense interest among the technologists and academia. In most rolling processes, the deformation geometries are designed such that the lateral spread of the work-piece is eliminated (or at least, minimised). Under such conditions, the problem becomes one of the solutions of plane strain field. Plane strain compression (PSC), therefore, is widely applied for the laboratory simulation of the rolling process[29], in the quest to understand effects of specific rolling conditions.

2.3 Plane Strain Compression (PSC)

Laboratory simulation of the rolling process is generally achieved by plane strain compression (PSC) deforming. The plane strain compression technique was first suggested by Orowan, in 1943, but successfully implemented by Ford in 1948[30]. The idea was a result of the increase in demand for determination of yield stress characteristics for strip material in the cold rolling process[17,30,31]. During the PSC deformation, the stored energy of the material increases up to a critical strain, which is often manifested through flattening of the stress-strain curve. For materials of relatively high SFE, such as aluminium, this generally signifies the strain for onset of steady-state recovery. The energy is generally depicted in terms of microstructural parameters, such as the subgrain size, the misorientation between the neighbouring subgrains and the internal dislocation density of the subgrains[29].

Deformation of a material is considered plane strain when there is no deformation in one axis, that is, when the deformation is biaxial. The extent of lateral spread of material during deformation is determined by the ratio of the workpiece width to the platen breadth (w/b). If the ratio is ≥ 5, then the material spread in the width (transverse) direction is negligible and this deformation is considered plane strain [24,32,33]. The other crucial geometric factor is the ratio of the platen breadth (b) to the specimen thickness (h), that is (b/h). This factor determines the strain distribution in the material. A typical PSC testing configuration is illustrated in Figure 2-3.

In the plane strain deformation process, strain localisation is not dependent on material properties but is constrained to regions that follow the theoretical slip line field. The field in turn depends on the geometry of the process. The slip line field changes instantaneously in line with the ever-changing ratio of the platen breadth to the specimen height (b/h)[34-36]. Figure 2-4 illustrates this concept. At high strains the number of crosses that indicate the slip line increases (i.e. b/h ratio increases) because of the specimen thinning. This results in a more homogeneous deformation being realised. This slip line approach generally holds at low friction levels.

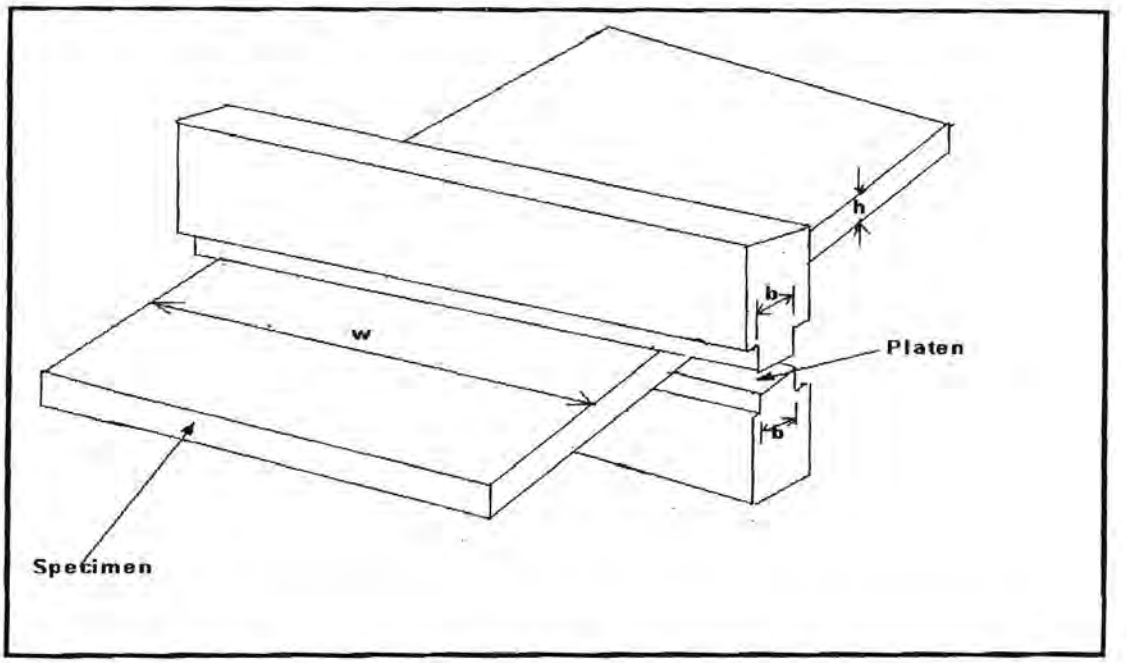

Figure 2-3. Schematic diagram of PSC test configuration

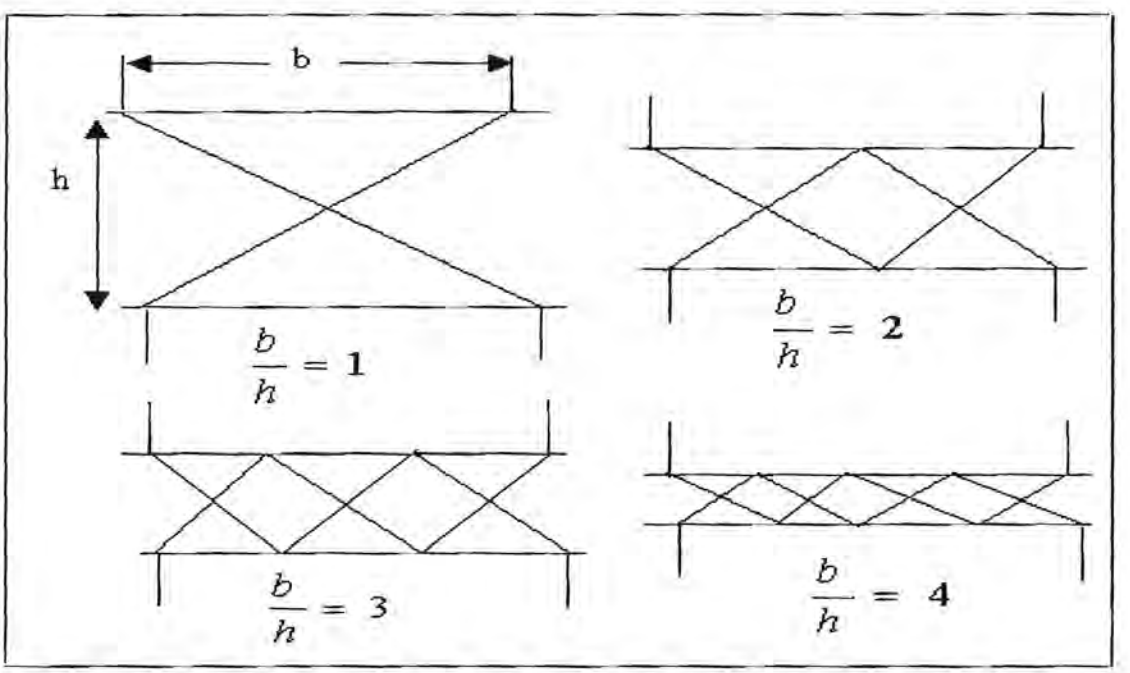

Figure 2-4. Slip-line distribution under frictionless PSC deformation

Plane strain compression testing allows the stress-strain behaviour of materials at elevated temperatures to be determined under controlled strain and strain rate. Figure 2-5 illustrates the schematic diagram of a PSC rig constructed by Duckham[34], at the University of Cape Town. The force limit of the rig is 250 KN under perfect working conditions. This allows the stress limit to be calculated from the Equation 2-4. From the formula, the dependence of the stress limit on the specimen as well as the platen geometry is clearly visible.

Stress limit = (250 kN) / (Contact Area)

Equation 2-4

The maximum strain rate of the equipment is determined by the crosshead speed of the equipment and the gauge length (or initial thickness) of the specimen; and is calculated according to Equation 2-5.

Strain rate = (Cross-head speed) / (Gauge length)

Equation 2-5

The maximum cross head speed for the specific rig is, nominally, $100ms^{-1}$.

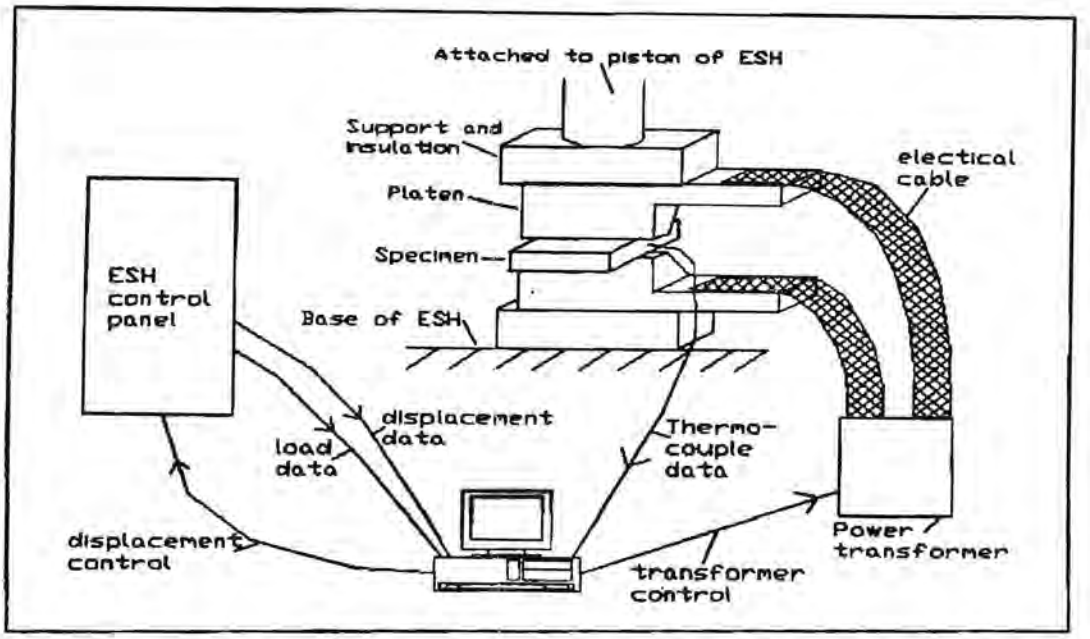

Figure 2-5. Schematic diagram of plane strain compression (PSC) rig[34].

2.4 Finite Element Modelling

Beynon and Sellars[35] and Colas and Sellar[36] have shown that the strain rates and strains are inhomogeneously distributed within the deforming zone. They invoke the slip-line theory to explain strain localisation, and they stressed the importance of the ratio of the platen breadth to the specimen thickness in determining the pattern and homogeneity of deformation.

Chen et al[37], in their thermomechanical model of hot rolling, noted that the volume fraction of material recrystallised and the size of recrystallised grains is dependent on the inhomogeneous deformations and the temperature distribution in the body being rolled.

In order to cater for the inhomogeneous distribution of strain through the thickness of the billet (plate) during rolling, Timothy et al[38] applied the concept of equivalent strain in their model of hot rolling. Equivalent strain simplifies the complex state of

strain encountered in the practical rolling situation by combining shear and compressive strains into a single parameter. They monitored the variation in equivalent strain through a slice of material in a deforming specimen and applied the same equivalent strains to simulate the rolling process using PSC.

Gasperini et al[39], postulate that the strain inhomogeneities, in a deforming body, are due to the presence of dislocation sheets that have undergone intense local shear (also known as *shear bands*). The shear bands tend to subdivide the deforming body into volumes, which are deformed by fewer slip systems. They applied boundary effects to explain the initiation of the initial microbands. The boundary effect is such that the normal stress decreases from the point of contact of the platen face and the deforming body on the surface to the centre of the body.

Mirza et al[40], also confirmed temperature, strain and strain rates inhomogeneities within the work-piece during rolling. By applying integrated finite element modelling, to simulate industrial roughing of AA3104, they managed to approximate the temperature and strain profiles across the plate thickness. They showed a significant temperature drop on the work-piece surface, for example from initial billet temperature of 730°C to 620°C during deformation. They attributed the fall in temperature to roll chilling. On the other hand, the centre of the plate showed a small increase or no change in temperature. Strain was also found to be highest on the surface and progressively decrease towards centre. However, for both temperature and strain, the gradients were found to be more prominent the thicker the work-piece, becoming more homogeneous with reduction in the stock thickness.

Of fundamental importance, however, is the fact that the through-thickness temperature and deformation inhomogeneities experienced by the work-piece on rolling are widely reported in literature[35-40]. To this end, laboratory simulations of industrial rolling processes that properly take into account these through-thickness variations give better approximation of the real process than those that assume

uniform nominal values. However, physical measurement of those parameters, in order to capture their distribution patterns, presents a technical and economic challenge. Finite element modelling, therefore, becomes a very handy tool for determining the approximate values of those varying parameters – e.g. temperature, strain, strain rate and stress.

The finite element method was first used in the metal forming field, to capture continuously varying parameters and material properties during processing, in the early seventies[41]. A finite element model (FEM) can be defined, simply, as a series of numerical techniques used in solving boundary value problems, initial value problems and eingenvalue problems.

The basic process in finite element modelling involves the discretisation (or division) of the actual geometry of the structure (or domain) into pieces, known as *elements*; approximation of the equations governing the problem for each element as function of selected values. The elements are joined together and boundary conditions are applied to selected values such that a solution can be obtained. Relevant equations are referred to during the numerical computations to obtain the approximate variables of the problem[41,42]. Each finite element represents a discrete portion of the physical structure, and the elements are linked together by nodes. The collection of nodes and finite elements forms a mesh and the number of elements in a particular mesh is known as the mesh density[40].

As computer aided engineering and design (CAE/CAD) gained momentum in manufacturing and processing, it became imperative, for computer engineers, technologists, and other stakeholders, to design user-friendly engineering simulation packages (or modules), such as ABAQUS. ABAQUS is a commercial suite of powerful engineering simulation programs based on the finite element method. It is designed as a general-purpose finite element modelling code capable of solving problems ranging from relatively simple linear analyses to most challenging non-linear simulations. It contains an extensive library of elements that

can model a wide variety of geometrical forms, as well as an extensive list of material models that can simulate most of typical engineering materials, including metals, rubber, polymers, composites, concrete, and geotechnical materials such as rocks and soils[41].

Chapter 3

3 EXPERIMENTAL METHODS

3.1 Material

3.1.1 Chemical Composition

The material of focus in this project is a commercial heat treatable aluminium alloy, AA6061. This is an Al-Mg-Si alloy with a chemical composition as given in Table 3-1.

	Si	Fe	Cu	Mn	Mg	Cr	Zn	Ti	Na	Ca	Bi	Al
LL	0.6	0.25	0.3	-	0.88	0.16	-	-	-	-	-	Bal
UL	0.8	0.35	0.4	0.14	1.12	0.24	0.22	0.1	0.004	0.003	0.004	

Table 3-1. Chemical composition of AA6061. (where: LL = lower limit wt.% and UL = upper limit wt.%)

3.1.2 History

The experimental material was supplied by Hulett Aluminium Rolled Products (Pty) Ltd.; based in Pietermaritzburg, South Africa. Samples were obtained from the commercial rolling process. The production of commercial rolled plates is achieved by thermomechanical processing of the cast slab as shown in Figure 3-1. First, a cast slab, of typical dimensions 5 m x 1 m x 0.62 m, is homogenised by soaking in a furnace at an elevated temperature of 525°C for at least 4 hours. From the furnace, the slab is charged into the hot roughing mill (HRM), where it is rolled down from a thickness of 620 mm to 26 mm, which is the transfer gauge thickness. The hot roughing is accomplished in 27 rolling passes conducted in a reverse fashion. During hot roughing, the temperature progressively decreases with time,

from 500°C to 370°C, since there are no re-heating steps included in the rolling process. After the HRM stage, the plate is transferred to the hot finishing mill (HFM), where it is further reduced to a specified thickness of 13 mm, commonly referred to as the finished gauge (plate). Although there is flexibility in the design of the HFM process schedule, a typical two-pass HFM schedule for producing 13 mm thick plate is presented in Table 3-2. Upon exit from the HFM, the finished plates are then coiled, and allowed to cool to room temperature prior to post-deformation processes, which are solution heat treatment, quenching, stretcher-levelling and ageing.

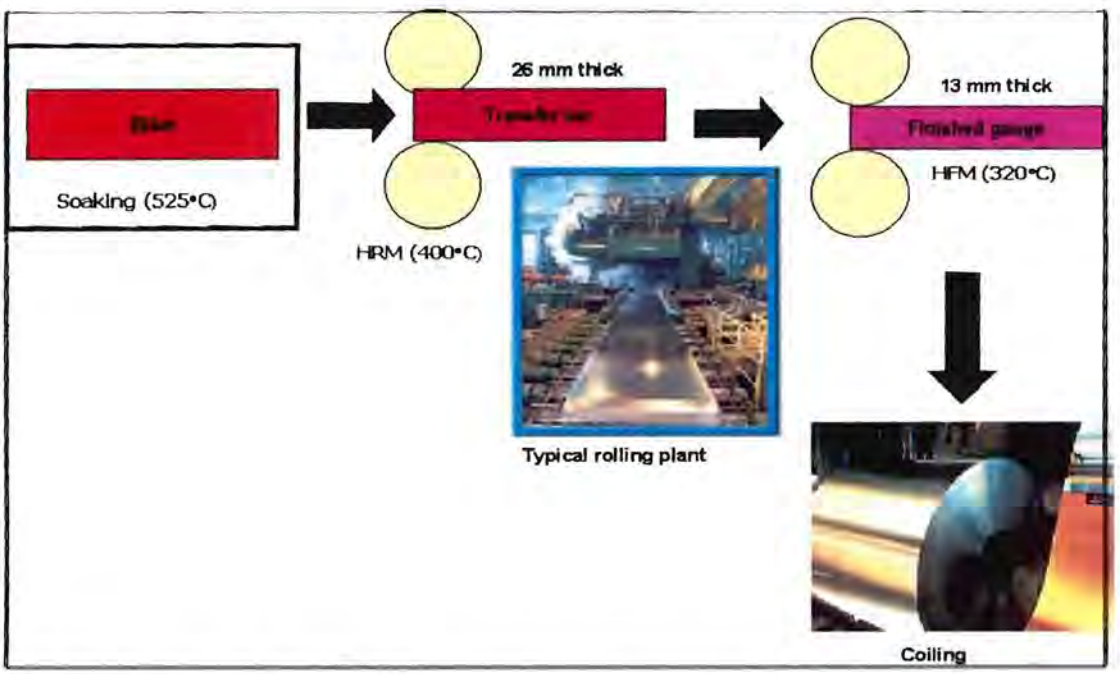

Figure 3-1. Schematic representation of a typical rolling process

HRM roller radius, r (m)	0.35

Pass	h_o (m)	h_f (m)	V_r (m/s)	ε	$\dot{\varepsilon}$ (s^{-1})	T (K)	Z (s^{-1})
1	0.02584	0.01599	1	0.55	9.44	365	5.25E+12
2	0.01599	0.01319	1	0.22	7.10	317	3.97E+13

Table 3-2. HFM process schedule for AA6061 13.19 mm thick plate.

The values of strain (ε), strain rate ($\dot{\varepsilon}$) and Zener-Hollomon parameter (Z) in Table 3-2 were calculated applying Equation 3-1, Equation 3-2 and Equation 3-3:

$$\varepsilon = 1.155\ln(h_o/h_f)$$

Equation 3-1

$$\dot{\varepsilon} = \varepsilon V_r/[r\,(h_o-h_f)]^{1/2}$$

Equation 3-2

$$Z = \dot{\varepsilon}\exp(Q/RT)$$

Equation 3-3

Where: h_o and h_f are the initial and final plate thickness, respectively; V_r is the roller velocity; r is the roller radius, Q is the deformation activation energy of the material; T is the absolute temperature of deformation and R is the gas constant.

Subsequent to HFM rolling, the plate is solution heat treated at 560°C for 10 to 20 minutes, followed by spray quenching to room temperature. After solution heat treatment and quenching, the plate is given a uniaxial tensile strain of 1 – 2 % to level the surfaces and relieve residual stresses, which may be present due to one or more of the preceding processes. Stretcher levelling, however, is known to have adverse effects on the material. Among the notable effects is the surface roughening phenomenon. Surface roughening has negative impact on the aesthetic and mechanical properties of the material[42,43]. After stretcher levelling, the plate is aged at 175°C for 8 hrs. This allows for the precipitation of Mg_2Si and other particles, necessary for improving the strength of the AA6061 alloy.

For these experimental studies, three different samples in the form of plates were provided, namely:

(1) Transfer gauge plate (tg)

This is a 26 mm thick plate, cut from the bulk plate just after the HRM, as shown in Figure 3-1. The material has only been subjected to 27 reverse-rolling passes, to reduce the cast slab from the initial thickness of 620 mm to 26 mm. The HRM processing was conducted within a temperature range of 400°C to 500°C. The plate was supplied in as-rolled condition. All the PSC specimens used in this project were machined from this transfer gauge sample, [see section 3.4].

(2) Heat treated finished gauge plate (fg_1)

This finished plate sample was supplied in the as-aged condition. The finished plate was obtained by further rolling of the transfer plate from 26 mm down to 13 mm thick in the HFM. Two HFM rolling passes are used to achieve the 13 mm gauge. The first pass was carried out at 365°C and the second pass at 317°C. Subsequently, the plate was subjected to post-deformation processes, namely solution heat treatment, quenching, stretcher levelling and ageing. The experimental sample was then cut from the bulk commercial heat-treated finished plate.

(3) As-rolled finished gauge plate (fg_2)

This finished plate sample was supplied in as-rolled condition. Sample fg_2 was cut from the finished plate just after the HFM stage, prior to post-deformation processes.

Therefore, samples fg_1 and fg_2 are differentiated by the fact that fg_1 was supplied after the usual commercial post-deformation processing described above, while fg_2 was supplied in the as-rolled state.

3.2 Microstructure Characterisation of Material

The main objectives of this project are to investigate the grain size sensitivity to thermomechanical process variables and influence of those variables on grain structure and/or hardness profiles that evolve through the plate thickness. To this end, metallographic studies have been carried out on the received commercial plates and on samples deformed in the laboratory using the PSC rig. In all cases, metallographic studies were done on the longitudinal plane; this is the plane containing the ND and RD, as shown in Figure 3-2(a).

In order to fully characterise the through-thickness grain structure profiles of commercially rolled plates, a series of micrographs were obtained, at slightly overlapping intervals, right through the thickness of the specimen; that is, from one surface to the other surface. Figure 3-2(b), for example, illustrates a situation where a total of five micrographs were taken at different positions represented by the coloured bands. Measurements were performed on those micrographs to characterise the through-thickness grain size profiles in the commercial plate.

In case of PSC deformed samples, grain size and hardness measurements were performed on the central part of the deformed zone, shown in Figure 3-4.

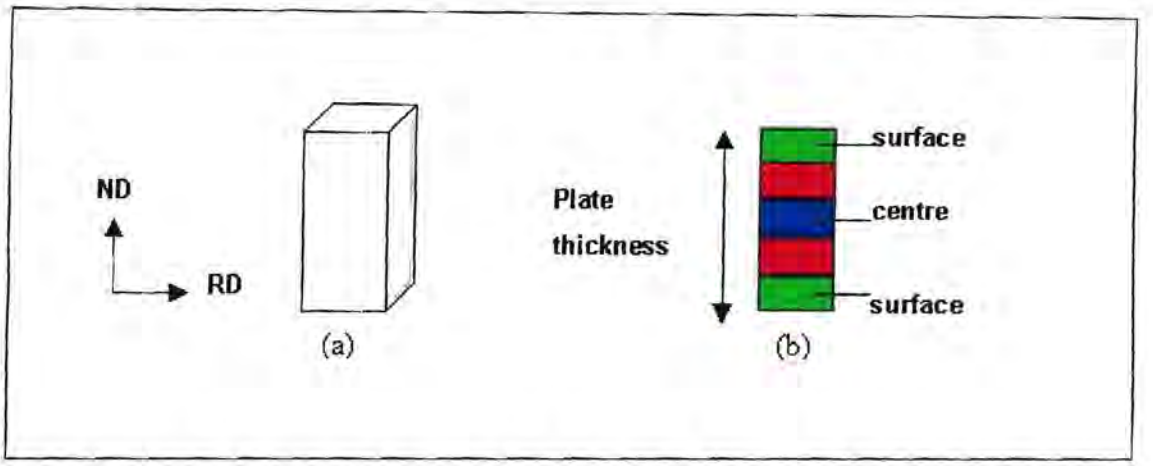

Figure 3-2. (a) shows the plane used for analyses; (b) illustrates through-thickness positions where metallographic pictures were taken.

3.2.1 Metallography Specimen Preparation

Specimens were cold mounted using a cold-mounting resin mixed with a curing agent in ratios 1:7 (hardener:resin). The mounted specimens were ground and polished using an automatic polisher, Struers Rotopol-22 fitted the Struers RotoForce-4. Method A from the Stuers Metalog Handbook[43] was applied with satisfactory results. In some instances, the specimens were ground and polished manually. In such cases silicon carbide grinding pads were used, with water as lubricant, starting from coarse 180 or 220 grit, and then progressing to finer grits up to the 1200 pad. Manual polishing was accomplished in three steps, commencing from 3 μm down to 1 μm and finally the 0.25 μm pad, using colloidal silica suspension (OPS) under a very light load. Polished specimens were then anodised using Barker's reagent, with a chemical composition of 46 ml HBF_4, 7 g H_3BO_3 and 970 ml H_2O. Anodisation conditions of 60 to 90 seconds, at room temperature and 20 V dc, achieved good results.

3.2.2 Microscopy

Metallograghic analyses of anodised specimens were conducted using a Reichert MeF3A polarised light microscope, operated in dark-field mode. The anodic layer deposited on the surface of the specimen is always anisotropic due to different grain orientations at the surface of the specimen. This allows grain contrast to be viewed on illumination with polarised light. Micrographs of the observed features were taken and used in the subsequent qualitative and quantitative analyses.

3.2.2.1 Grain Size Determination

The standard linear intercept method was used to measure grain sizes on the optical micrographs. The grain structure was highly anisotropic, with grains typically elongated in the rolling direction (RD). Therefore, mean grain sizes were determined for the RD, that is longitudinal diameter (D_L) and/or the ND, which is short-transverse diameter (D_T). Each grain size value is an average from counting the number of grains intercepted by at least ten lines drawn right across the given micrograph, in the ND or RD. The grain sizes were calculated from the relationships given in Equation 3-4 and Equation 3-5, below:

$$P_L = PM/L_T$$

Equation 3-4

$$D = 1/P_L$$

Equation 3-5

Where P is the number of grains intercepted by the lines, L_T is the length of the lines and M is the magnification. P_L is the number of intersections per unit length. D is the mean linear intercept length (or the grain diameter).

3.2.3 Particle Distribution

Optical microscopy was applied to perform qualitative analysis of the through-thickness particle distribution. The transfer and finished plates were investigated in the as-rolled condition. Presence of through-thickness particle distribution gradients would be expected to affect the microstructure and mechanical property homogeneity through the plate. The exercise was intended to assess whether certain grain size and hardness trends could be attributed to particle distribution patterns. The specimen mounting, grinding and polishing procedures were identical to those described in section 3.2.1. A series of micrographs, were obtained right through the plate thickness, at slightly overlapping intervals and the surfaces were analysed in the as-polished condition - no prior etching or anodising. The Reichert MeF3A microscope, operated in the bright-field mode, was used in this analysis.

3.3 Hardness Testing

Macrohardness measurements were carried out on all the supplied plates, as well as some of the PSC specimens. Samples were tested in the as-rolled state and after heat treatments. For purposes of monitoring hardness gradients in commercial plates, hardness values were systematically measured right through the plate thickness in the ND, with indentation spacing of ~2 mm. All recorded hardness values are averages from four indentations. The standard Vickers hardness (HV) test, which uses a four-sided pyramid shaped diamond indenter, was used through out this project work. The machine used was an ESE-WAY, SPVR.2.M model, fitted with an optical microscope. The diagonals of the resultant indentations are measured under the microscope and the corresponding hardness values are read from conversion tables. The machine also allows the size of the indentation load to be selected and a load of 30 kgf was applied throughout this work.

3.4 Effects of Thermomechanical Process Variables by PSC

The plane strain compression (PSC) rig used in this work was designed and built by Duckham[32]. The rig is capable of producing an output load of 250kN, a crosshead speed of 100 $mm.s^{-1}$ and a strain rate of $10s^{-1}$ when using a 10 mm thick specimen. However, nominal strain rates encountered in HFM, as calculated from rolling schedules provided by industry, are mostly above $10s^{-1}$. To comply with the rig design limits, such rolling schedules were simulated using the Z parameter. In which case the strain rates and the corresponding temperatures were adjusted such that the Z values were maintained equal to those encountered in industry.

The PSC technique allows controlled variation of thermomechanical variables – temperature (T), strain (ε), strain rate ($\dot{\varepsilon}$) and the Zener-Hollomon parameter (Z). PSC is hence a useful research tool for laboratory simulation of industrial rolling processes. Generally, thermomechanical processing has a critical effect on the microstructure and property evolution in the material. However, it has also been observed[45] that, in the rolling of AA6061, the HFM operations have much more profound influence on the final plate properties as compared to HRM history. Therefore, this work focuses on simulating only those conditions encountered in HFM processing of the AA6061 alloy.

A range of 1-pass and 2-pass PSC tests were conducted on transfer gauge specimens measuring 52 mm x 33 mm x 10 mm. The specimens were machined from any section of the bulk material, since the characterisation of the transfer gauge plate, also done as part of this project work, has not shown any significant variations in through-thickness grain structure and hardness. Thus, it did not really matter from which section of the plate the PSC specimen was obtained. The specimen orientation, relative to the plate geometry, was always such that the simulated rolling direction was parallel to the original rolling direction of the plate,

as shown in Figure 3-3. Prior to the PSC testing, the samples were ground to a smooth surface finish, using a 1200 grit SiC paper, and coated with a layer of graphite lubricant. The lubrication method was reported by Shi et al[43] to be effective in reducing the coefficient of friction between the work-piece and the platens.

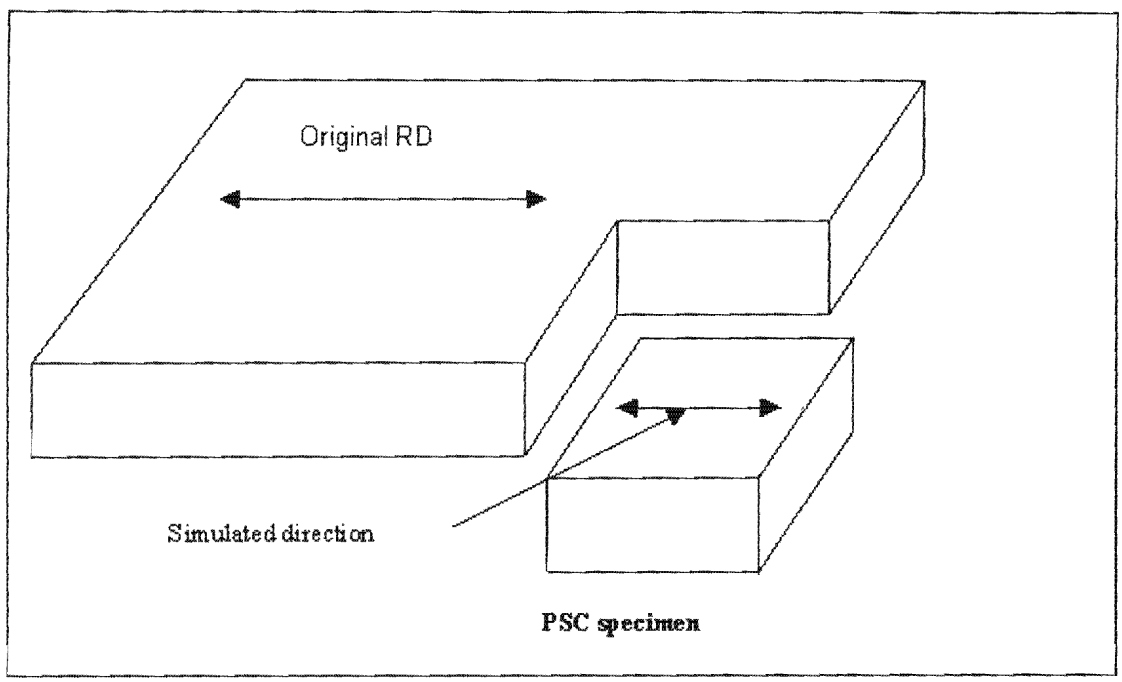

Figure 3-3. PSC specimen orientation relative to actual RD[34].

The PSC rig is coupled to a computer, which has a program that prompts the operator to enter the deformation test parameters: contact area, initial thickness of the specimen (h_o), reduction distance, strain rate, temperature, number of passes and interpass time. When deformation is finished, the platens automatically separate, enabling manual gripping (using tongs) and quenching of the specimen in cold water. Figure 3-4 shows a schematic diagram of the deformed specimen.

During deformation the load, temperature and displacement data are collected by the computer in form of voltage signals and then processed to generate outputs in more usable forms, such as true stress [MPa], temperature [°C] and true strain.

The true stress (σ) and true strain (ε) are computed from the von Mises stress and strain criterion, and they are given by Equation 3-6 and Equation 3-7, respectively.

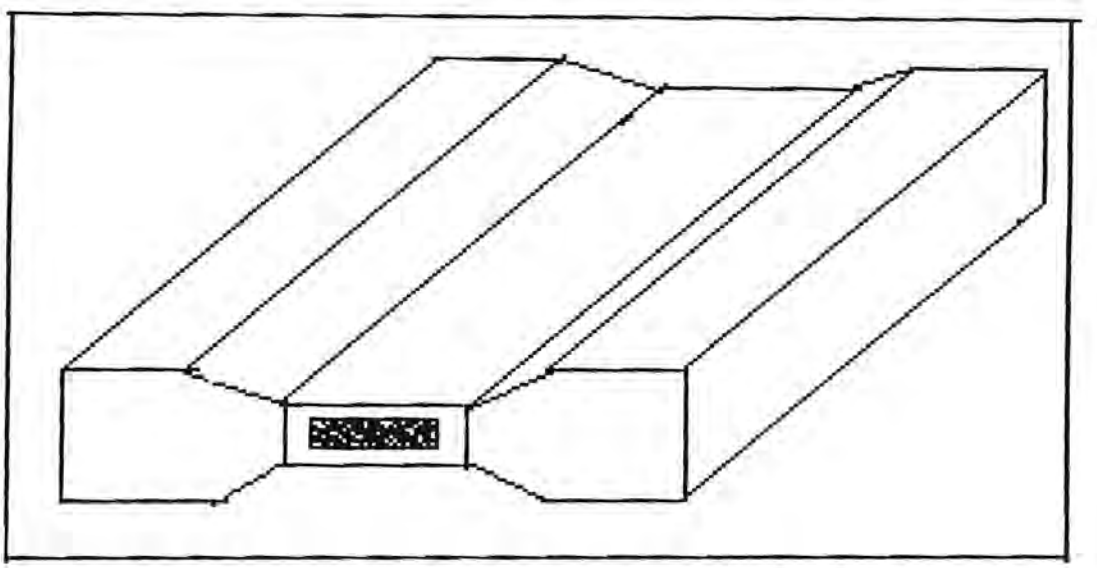

Figure 3-4. Schematic diagram of PSC specimen

$$\sigma = (1/1.155)(\text{load/area})$$

Equation 3-6

$$\varepsilon = 1.155\ln(h_o/h_f)$$

Equation 3-7

Where: h_o and h_f are the thickness of the specimen before and after deformation respectively.

Note that for all subsequent analyses on the PSC deformed specimens, only the central portion of the deformed zone, which is the *shaded area* in Figure 3-4, was used. Furthermore, for the purposes of this study, deformation was assumed to be uniform throughout the shaded cross-section.

The PSC simulations were mainly confined to single-pass schedules to minimise or eliminate complexities (or ambiguities) associated with multi-pass simulations, such as, inter-pass time and varying conditions for each pass. A few two-pass simulations were included though. During two-pass deformation the specimens are heated to the specified first deformation temperature, deformed and then allowed to cool to the second deformation temperature while held by the platens, followed by deformation and then quenching to room temperature. Details of the experimental matrices used in the PSC tests are as shown in Table 3-3 to Table 3-6. The variable matrices were carefully selected to incorporate some currently practised industrial rolling schedules and proposed potential schedules.

1-pass PSC Simulations: @ Varying T and Z; and Constant ε and $\dot{\varepsilon}$.				
Test No.	**ε**	**$\dot{\varepsilon}$ [s^{-1}]**	**T [°C]**	**Z [s^{-1}]**
1	0.8	10	**211**	**2.0E+16**
2	0.8	10	**246**	**1.9E+15**
3	0.8	10	**271**	**4.2E+14**
4	0.8	10	**303**	**7.5E+13**
5	0.8	10	**344**	**1.1E+13**
6	0.8	10	**368**	**4.0E+12**

Table 3-3. PSC matrix for investigating effects of T or Z

1-pass PSC Simulations: @ Varying ε; and Constant $\dot{\varepsilon}$, T and Z.				
Test No.	**ε**	**$\dot{\varepsilon}$ [s^{-1}]**	**T [°C]**	**Z [s^{-1}]**
1	**0.2**	7.5	365	2.9E+12
2	**0.2**	7.5	365	2.9E+12
3	**0.6**	7.5	365	2.9E+12
4	**0.8**	7.5	365	2.9E+12
5	**1.0**	7.5	365	2.9E+12

Table 3-4. PSC matrix for investigating effects of strain (ε)

1-pass PSC Simulations: @ Varying $\dot{\varepsilon}$ and T; and Constant ε and Z.				
Test No.	ε	$\dot{\varepsilon}$ [s^{-1}]	T [°C]	Z [s^{-1}]
1	0.8	**2**	**276**	7.45E+13
2	0.8	**5**	**288**	7.45E+13
3	0.8	**7.5**	**296**	7.45E+13
4	0.8	**10.8**	**303**	7.45E+13

Table 3-5. Matrix for investigating effect varying $\dot{\varepsilon}$ and T keeping Z constant

2-pass PSC simulations						
Test No.	Pass No.	T [°C]	ε	Total ε	$\dot{\varepsilon}$ [s^{-1}]	Z [s^{-1}]
1	1	**288**	0.6	0.9	10	**1.6E+14**
	2	**276**	0.3		10	**3.1E+14**
2	1	**330**	0.6	0.9	10	**2.0E+13**
	2	**291**	0.3		10	**1.4E+14**
3	1	**340**	0.6	0.9	10	**1.3E+13**
	2	**300**	0.3		10	**8.6E+13**
4	1	**353**	0.6	0.9	10	**7.3E+12**
	2	**304**	0.3		10	**7.1E+13**
5	1	**365**	0.6	0.9	10	**4.5E+12**
	2	**317**	0.3		10	**3.7E+13**

Table 3-6. 2-pass PSC matrix

Having established the sensitivity of the grain structure and hardness properties to temperature, strain and strain rate, the next key issue of this project was to predict the distribution of these variables through the plate thickness during rolling. Ultimately the prediction of through-thickness variable distributions coupled with the experimental knowledge of the influence of each of the variables on the grain size and hardness properties, would allow the through-thickness grain structure and mechanical property profiles to be predicted as well. To this end, a finite element model (FEM), whose purpose was to calculate the temperature and strain distribution though the plate thickness, was designed using the commercial package ABAQUS/Explicit, Version 6.2.1.

3.4.1 Finite Element Modelling

The rolling process can be regarded as an initial value problem since the material response to deformation is generally governed by its initial conditions, such as temperature differentials between work-piece and its environment, elastoplasticity and viscoplasticity, among others. In this case, deformation was assumed to be viscoplastic, a commonly acceptable assumption in modelling processes in which plastic deformation is much larger than the accompanying elastic deformation. The assumption simplifies the problem formulation and makes computation much more economic, without significantly compromising the accuracy of solutions. The rolling process is also considered symmetrical about the centre of the plate, hence only the upper roller and half the plate (that is from surface to centre) were modelled

In designing a FEM it is critical to decide on the output data required from the model, and then define the numerical model accordingly. In this particular case, strain and temperature distributions through the plate thickness were the main focus. The FEM input-deck was generated using the commercial package ABAQUS/Explicit module. The problem was defined by applying standard coding specified for two-dimensional (2D), four-noded plane strain continuum elements[42]. The modelling consists of two critical parts (or models) coupled together - the thermodynamic model and the mechanical model.

3.4.1.1 Thermodynamic Model

The three major means of heat transfer - conduction, radiation and convection – to and from the plate and the roller as well as the environment - were modelled by incorporating the appropriate heat transfer coefficients into the model. Heat exchange was assumed to take place from the contact surface of the work-piece, since losses from the sides of the plate are expected to be much smaller than the surface, which has a much larger cross-sectional area. The values for all heat transfer coefficients were taken from literature[1,2,42]. The roller was assumed to be

isothermal and set at a constant temperature of 150°C. It is well known that the temperature of the roller varies during rolling; however, trying to model the thermal behaviour of the roller would have required a very fine meshing of the roller in order to define the curved surface accurately enough to minimise the roll noise. This would have greatly increased the computational expense, and yet it was felt that such detailed modelling of the roller was not likely to result in significant improvement to the accuracy of the model. Heat transfer by radiation and convection phenomena were incorporated into the model using the following equations[42,48]:

Radiation heat transfer to the environment was modelled using Equation 3-8:

$$Q_{radiation} = \varepsilon_r \gamma[(T-T_Z)^4-(T_O-T_Z)^4]$$

Equation 3-8

Convection heat transfer to the environment was modelled by Equation 3-9:

$$Q_{convection} = -h(T-T_O)$$

Equation 3-9

Where: ε_r = material surface emissivity , γ = Stefan-Boltzmann constant, T = material temperature, T_O = environment temperature, T_Z = Absolute zero temperature, and h = coefficient of convection heat transfer.

Heat generated by plastic work was also modelled by Equation 3-10:

$$r^{pl} = \eta\sigma : \dot{\varepsilon}^{pl}$$

Equation 3-10

Where: r^{pl} denotes the heat flux added to the thermal energy balance, σ is the stress matrix, $\dot{\varepsilon}$ is the strain rate and η is a coefficient defined by the user. Note

that the colon represents the sum of the matrix conjugate products. Specific heat was also incorporated in the model.

3.4.1.2 Mechanical modelling.

The model was constructed as a single-pass process, which relatively simplifies the problem definition and computation process, as compared to a multi-pass process. A multi-pass model is complicated by the fact that different conditions - temperatures, strain rates and strains - vary from one pass to another, within the same rolling schedule. Incorporating several passes in a one input-deck would require the model to have several loops in order define initial and boundary conditions for each and every pass. This was attempted and found to present some computational problems. Finally, simulation of multi-pass schedules was carried out using a series of 1-pass runs. The plate had to be re-meshed and new material data, such as flow stress curves, had to be entered after each preceding pass. The plate was modelled using 205, 4-noded plane strain continuum elements. The elements where numbered, starting form the bottom row (centre of the plate) and from the right to the left, as shown in Figure 3-5. All FEM output data was taken from the mid-length elements, these are 21, 62, 103,144 and 185. The position was chosen to minimise noise, which is generally more pronounced at the ends of the plate, particularly as it enters or leaves the roll-gap. The initial plate dimensions (that is plate geometry at the beginning of pass 1) used were 90 mm x 13 mm (length x thickness). (The typical input-deck used for the simulation is given in appendix 1).

205	204	203	-	-	-	-	-	-	-	-	-	**185**	-	-	-	-	-	-	-	-	-	167	166	165
164	163	162	-		-	-	-	-	-	-	-	**144**	-	-	-	-	-	-	-	-	-	126	125	124
123	122	121	-	-	-	-	-	-	-	-	-	**103**	-	-	-	-	-	-	-	-	-	81	82	83
82	81	80	-	-		-	-	-	-	-	-	**62**		-	-	-	-	-	-	-	-	40	41	42
41	40	39		-	-	-	-	-	-	-	-	**21**	-	-	-	-	-	-	6	5	4	3	2	1

Figure 3-5. Modelled mesh, showing the element numbering and through-thickness position where FEM output data were obtained.

The roll velocity conditions were taken from commercial rolling schedules provided by the industry. The plate was always given an initial velocity, equal to the x-component of the roller, in order to minimise the shock force on the roller and the plate at the point of entry into the roll-gap.

The roller was modelled as a rigid body (analytical rigid surface) as it was realised that the deformation of the relatively much softer AA6061 alloy, under hot rolling conditions, would not result in any significant deformation of the much more stiffer steel rollers.

The basic Coulomb friction model was used with specified maximum value of friction before shearing of the work-piece material took place. Plastic flow stress curves of the material were obtained from PSC stress-strain curves. So, PSC tests were initially done using nominal rolling schedule conditions, and the output stress-strain data were subsequently used as material behaviour inputs into the FE model. The sets of stress-strain data were always grouped in ascending order. The program interpolated the material behaviour between given points by assuming a linear relationship. Furthermore, the program also assumed a steady state flow stress condition after the last data point entered[42]. The material properties were assumed to be isotropic throughout the simulation.

Chapter 4

4 RESULTS

4.1 Characterisation of Industrial-Rolled Plates

4.1.1 Microstructure of Supplied Plates

Figure 4-1 shows micrographs of the transfer and finished plates in the as-rolled condition. No grain-size information can be discerned from the optical micrographs. Only continuous deformation bands, parallel to the rolling direction, are observed in both cases. Very similar deformed structures were revealed through out the thickness of the individual plates.

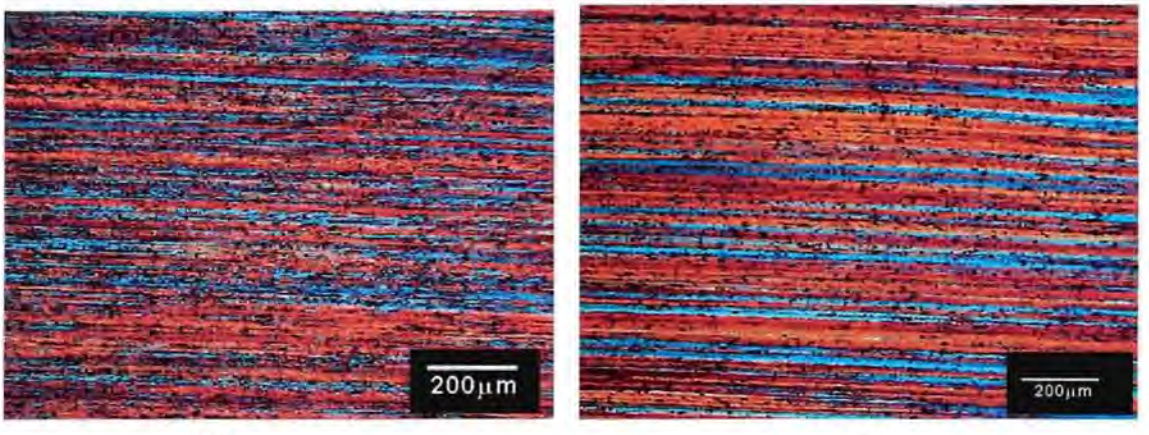

(a) (b)

Figure 4-1. Micrographs from as-rolled (a) transfer plate (tg) and (b) finished plate (fg2). The microstructures reveal some deformed bands parallel to the RD, however, no grain size information can be discerned.

Figure 4-2 (a) – (b) show microstructures of the surface and centre positions of laboratory heat-treated transfer plate.

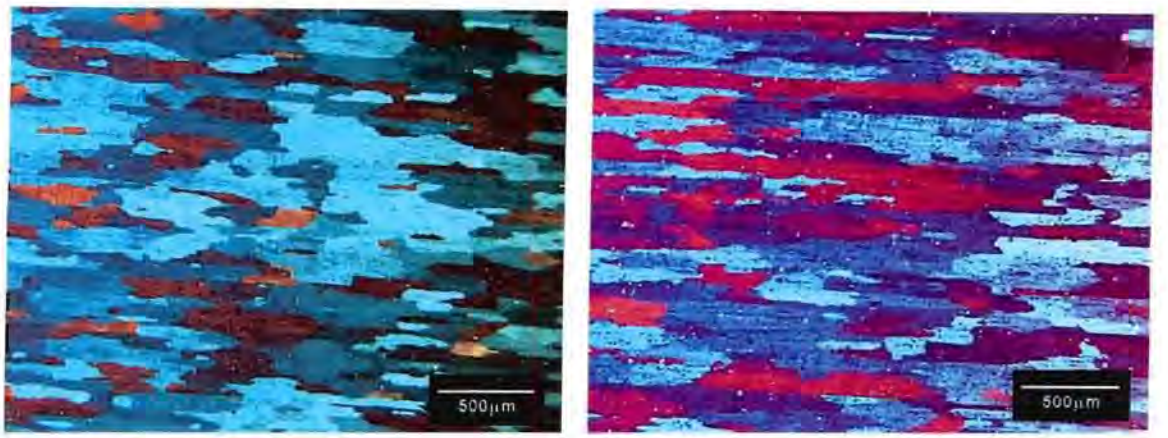

(a) D_T = 78±2 μm & D_L = 347±1 μm **(b) D_T = 75±3 μm & D_L = 333 ±2 μm**

Figure 4-2. Grain structure for (a) the surface and (b) centre positions of transfer plate thickness; specimens were analysed in the aged condition.

The grains are typically flat, and elongated in the rolling direction. Applying the standard linear intercept method, grain sizes for the centre and surface positions of the plate thickness were calculated to be: (a) for the plate surface, D_T = 78±2 μm and D_L = 343±2 μm; giving a grain aspect ratio (D_L/D_T) ~4.4 and (b) for the centre, D_T = 75±3 μm and D_L = 333±2 μm; giving a grain aspect ratio (D_L /D_T) ~4.4. The overall mean grain sizes through the plate thickness were calculated to be D_T = 77 μm and D_L= 338 μm. It is observed that the grain sizes for the centre and surface of the plate are very similar (or are rather marginally different). On the strength of these observations, the grain structure of this transfer plate can safely be regarded as uniform through the thickness. This means, from grain structure point of view, the PSC specimens could be machined from any position through the plate thickness. However, in this study the specimens were machined in such a way that the 26 mm thick transfer plate sample was first sliced through its mid-thickness, in the transverse direction, into two 13 mm thick plates. Then the standard PSC specimens (section 3.4) were then machined from the two 13 mm thick plates.

Figure 4-3 (a) – (b) show microstructures of the surface and centre positions, respectively, of commercial rolled and heat-treated finished gauge (fg_1) plate

Through-thickness transverse grain size gradient is observed in this plate, with the grain size progressively decreasing from the surface (D_T = 65 ±3 μm and D_L = 347± μm) to the centre (D_T = 51±4 μm and D_L = 338± μm). The short-transverse grain size (D_T) of the surface microstructure is found to be approximately 1.3 times that of the centre. The grain morphology remains flat and elongated in the rolling direction. The overall average through-thickness grain sizes were calculated to be, D_T = 60 μm and D_L = 341 μm.

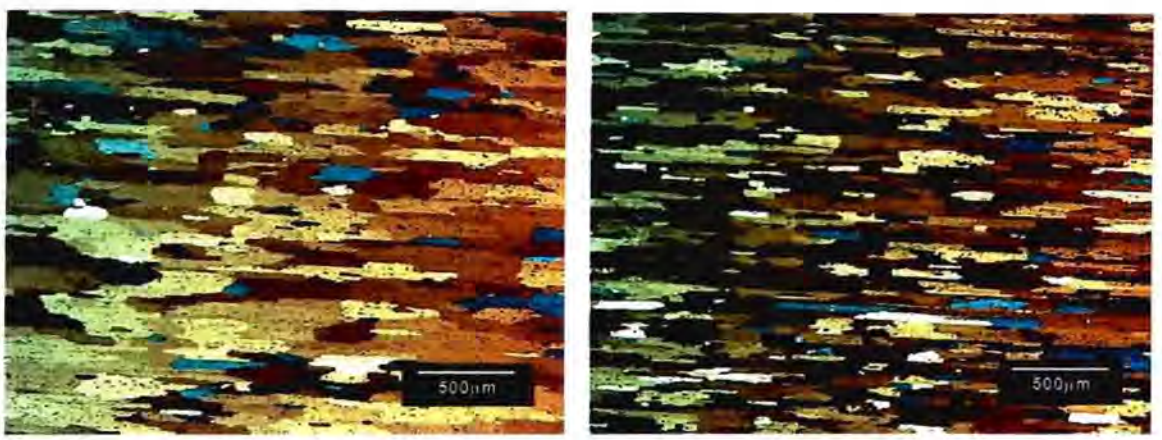

(a) D_T = 65±3 μm and D_L = 347±1 μm **(b) D_T = 51±5 μm and D_L = 338±3 μm**

Figure 4-3. Grain structure for (a) the surface and (b) centre positions of finished plate (fg_1) thickness; supplied in the as-aged state.

Table 4-1 summarizes the quantitative recrystallised grain size data from the supplied transfer and finished plate micrographs. (Typical standard deviations encountered in this study are also included in the table; the standard deviations were generally ≤ 5 μm.

Material	Through-thickness position	Grain size		Aspect ratio
		D_L [μm]	D_T [μm]	D_L/D_T
Transfer gauge:(tg)	Centre	**333±2**	**75±3**	4.4
	Surface	**343±1**	**78±2**	4.4
Finished gauge 1: (fg_1)	Centre	**338±3**	**51±5**	6.6
	Surface	**347±1**	**65±3**	5.3

Table 4-1. Mean longitudinal (D_L) and short-transverse (D_T) recystallised grain sizes for the surface and centre positions of the supplied plates.

4.1.2 Vickers Hardness (HV) for Supplied Plates

Figure 4-4 to Figure 4-6 depict through-thickness Vickers hardness (HV) profiles for the transfer and finished (fg_1 & fg_2) plates, tested in different conditions (tempers) - that is, as rolled, solution heat-treated and solution heat-treated plus aged conditions. The hardness for both transfer and finished plates, in the as-deformed state, do not show any variation through the plate thickness. The overall average hardness values are 48 ± 1 for the transfer plate and 52 ± 1 for the finished plate. The uniform through-thickness hardness suggests either even distribution of dislocations through the thickness or the deformation gradients may be present on such a scale that cannot be detected by hardness test. Thus, the grain size gradient observed in the finished plate microstructure, Figure 4-3, may not necessarily be due to stored energy differentials through the plate. Other metallurgical and/or thermomechanical phenomena could be responsible. Particle distribution gradients are a potential cause for grain size differences. A region with a higher concentration of second phase particles would result in a finer grain structure due to relatively higher pinning effect. This particle distribution through the plate thickness was investigated. However, particle distribution analysis, by optical microscopy, as depicted in section 4.1.3, did not reveal any definitive trends.

Further, it is observed, in Figure 4-6, that the hardness profile curve for the as-rolled finished plate (fg_2) is slightly above that of the transfer plate (tg). This meets with the expected increase in dislocation density (stored energy) resulting from the additional strain, to which the finished plate has been subjected in the HFM. Moreover, the HFM processing is conducted at relatively lower temperatures, which results in less dislocation recovery occurring, and hence the slight increase in hardness.

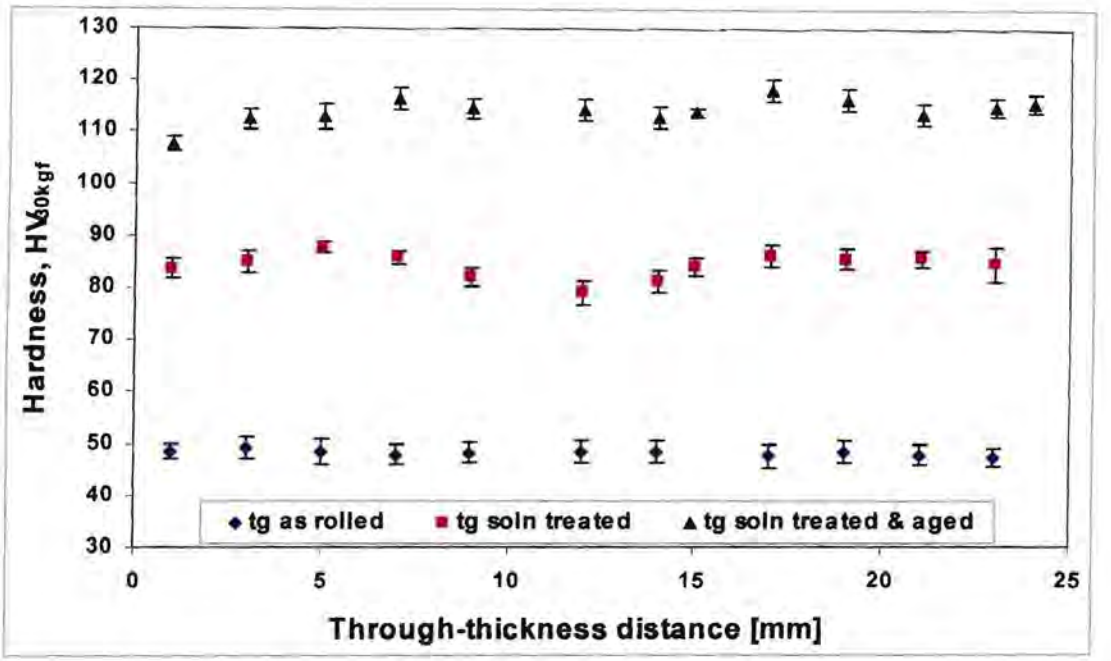

Figure 4-4. Hardness profiles for transfer plate (tg); tested in (a) as-rolled, (b) solution heat treated, and (c) solution heat treated & aged state.

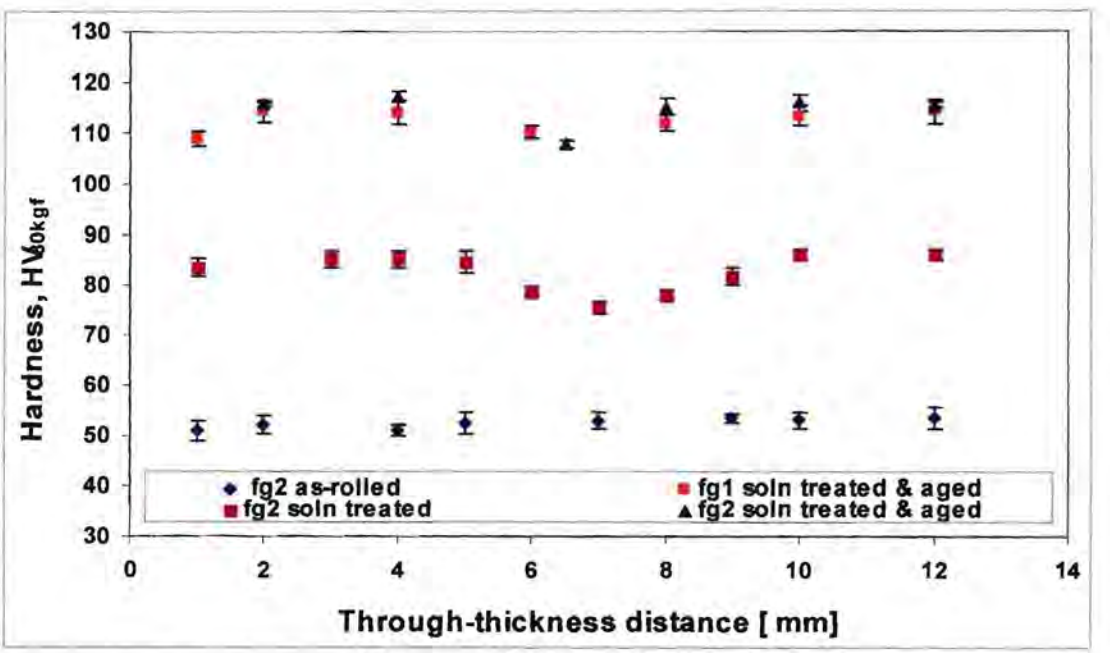

Figure 4-5. Hardness profiles for finished plates - fg_1 and fg_2.

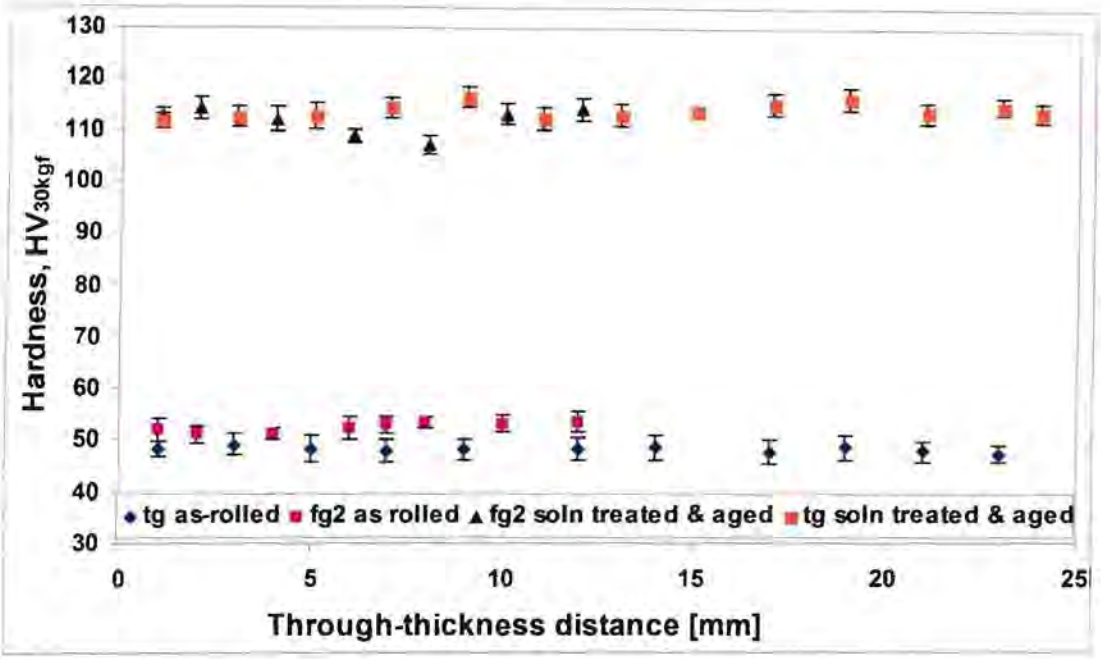

Figure 4-6. Comparison of hardness profiles for transfer and finished plates - tg and fg_2.

Slight through-thickness hardness variations are observed in all the individual heat-treated plates, fg_1, fg_2 and tg, Figure 4-4 to Figure 4-6. Interestingly, in all cases, the hardness profiles show minima just about the mid-thickness of the plate. The phenomenon is more pronounced in those specimens tested after solution heat treatment and quench only, and less so in those that have been subjected to solution heat treatment, quenching and ageing.

No significant differences in hardness are observed in all heat-treated specimens – from transfer and finished plates - despite notable grain size differences observed in their microstructures, Figure 4-2 and Figure 4-3. In fact, the hardness profiles for heat-treated finished and heat-treated transfer plates are more less a duplicate each other, Figure 4-6. This either suggests that grain size does not significantly influence the mechanical strength of AA6061 or that the relative grain size difference of about 20%, in this particular case, is not large enough to give any detectable impact. However, it is also observed that the hardness increases

significantly with heat treatment processes. This clearly indicates that solid solution and precipitate hardening are the predominant strengthening mechanisms in this material.

Grain size may not have a significant effect on the mechanical strength of aluminium alloys, or at least in AA6061 especially, as can be inferred from the above hardness and microstructure analyses. However, grain size is also known to influence a host of other material properties, such as creep resistance, corrosion and surface roughening. Therefore, grain size control still remains a critical technological issue in most materials.

4.1.3 Through-thickness Particle Distribution

Figure 4-7 and Figure 4-8 show series of optical micrographs obtained from different positions through the thickness of as-rolled plates – tg and fg_2. Particle distribution gradients are a potential cause for grain size differences, observed in section 4.1.1. A region with a higher concentration in second phase particles would result in a finer grain structure due to a stronger pinning effect of the particles. However, optical microscopy did not reveal any consistent particle distribution gradients. The particle distribution gradients may be present on such a fine scale, which requires other techniques with a better resolution. These results alone are not conclusive with regards to whether specific particle distribution patterns exist through the plate thickness or not. This may need further exploration.

In fact, Figure 4-7(a) actually suggests a finer particle distribution on the surface of the plate, but this would be contrary to the observed trends in grain size in the finished plate, i.e. coarser grain size at the plate surface.

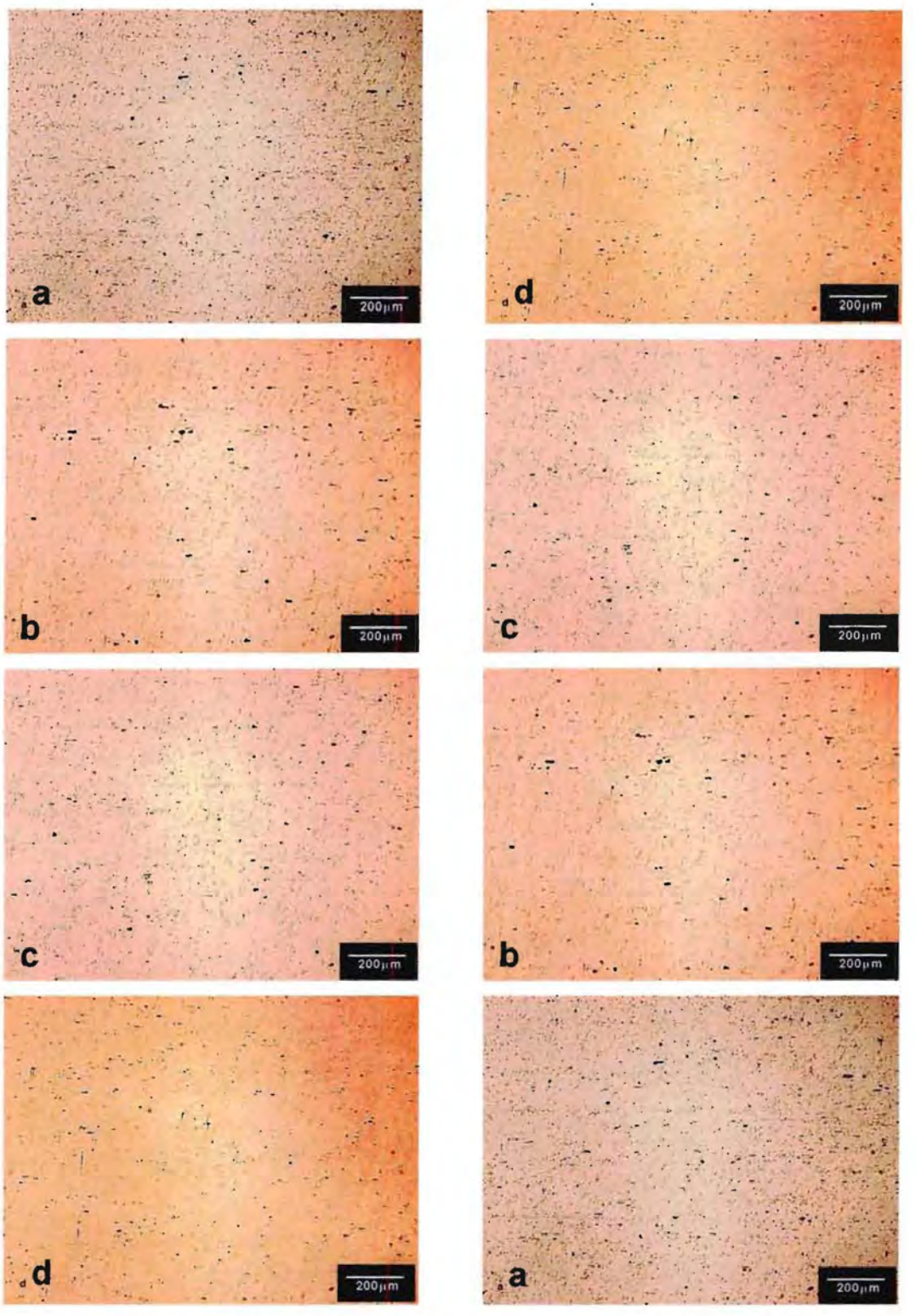

Figure 4-7. Through-thickness particle distribution in the transfer plate; from surface (a) to centre (d). The two columns are just for ease comparison.

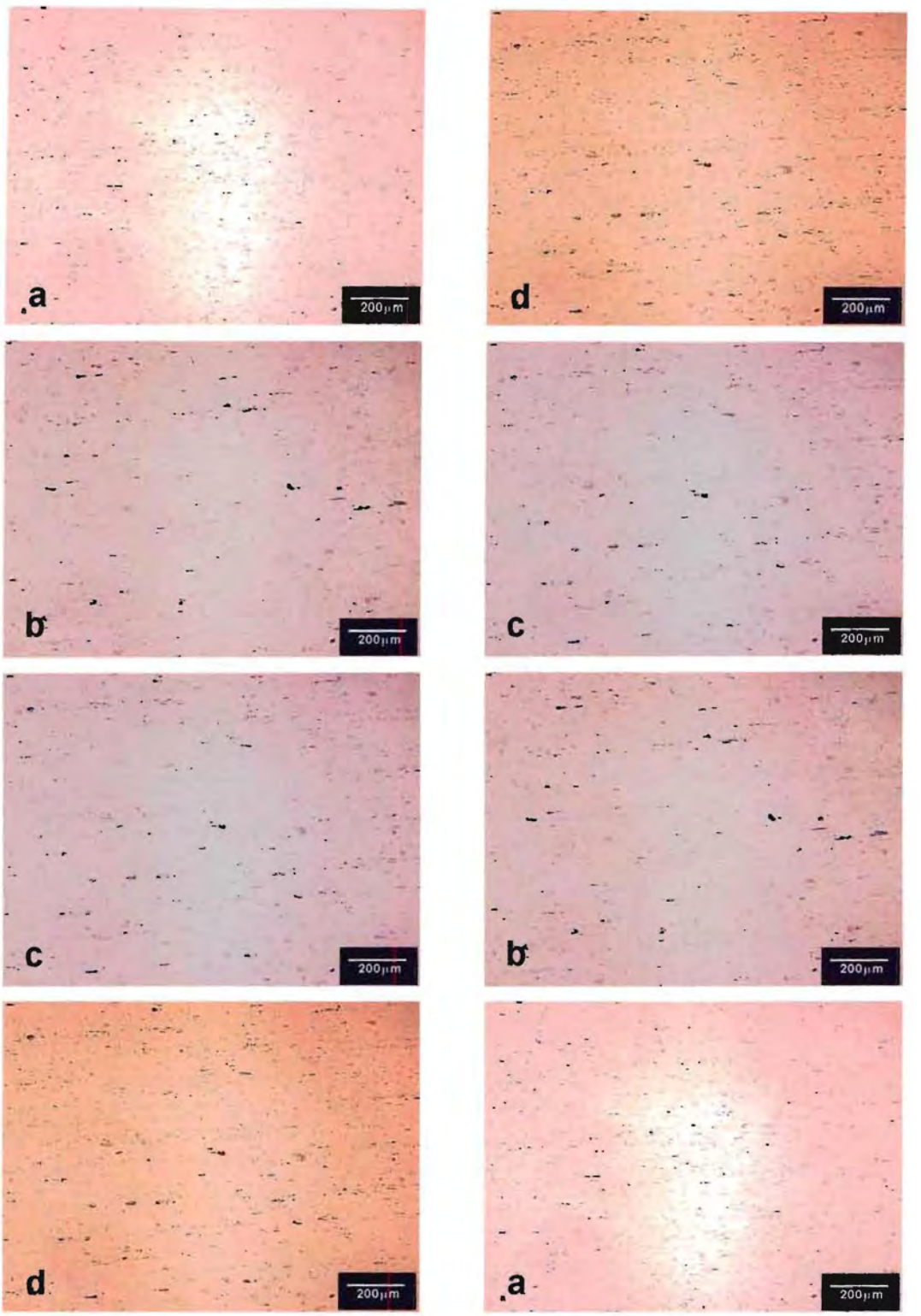

Figure 4-8. Through-thickness particle distribution in finished plate; from surface (a) to centre (d). No definitive distribution pattern is manifested.

4.2 PSC Testing

The PSC rig enables setting and controlling of rolling variables – T, ε, $\dot{\varepsilon}$ and Z – and key outputs of the PSC testing are the true stress-strain values, which are readily available after testing. Figure 4-9 shows plots of true stress versus true strain data for six one-pass simulations carried out at different temperatures, ranging from about 200°C to 370°C. A constant strain rate of $10s^{-1}$ was used in all the six cases; hence, the Z-parameter is only varying with temperature. By comparing the graphs, it can be observed that, the flow stress decreases as deformation temperature increases. In addition, the plots indicate, that the flow stress, in all cases, approaches a steady state condition. The steady-state situation is also attained faster with increase in deformation temperature, indicating higher dynamic recovery rates at higher temperatures.

Understanding the stress-strain behaviour of a material under given processing conditions is a critical aspect in material processing. For this project, in particular, the stress-strain data depicted in these curves, Figure 4-9, are part of the prerequisite input information for modelling the material behaviour. Actually, the data form the basis for further numerical computation of the through-thickness strain and stress distribution by the finite element model (FEM). More stress-strain curves are given in Appendix 2

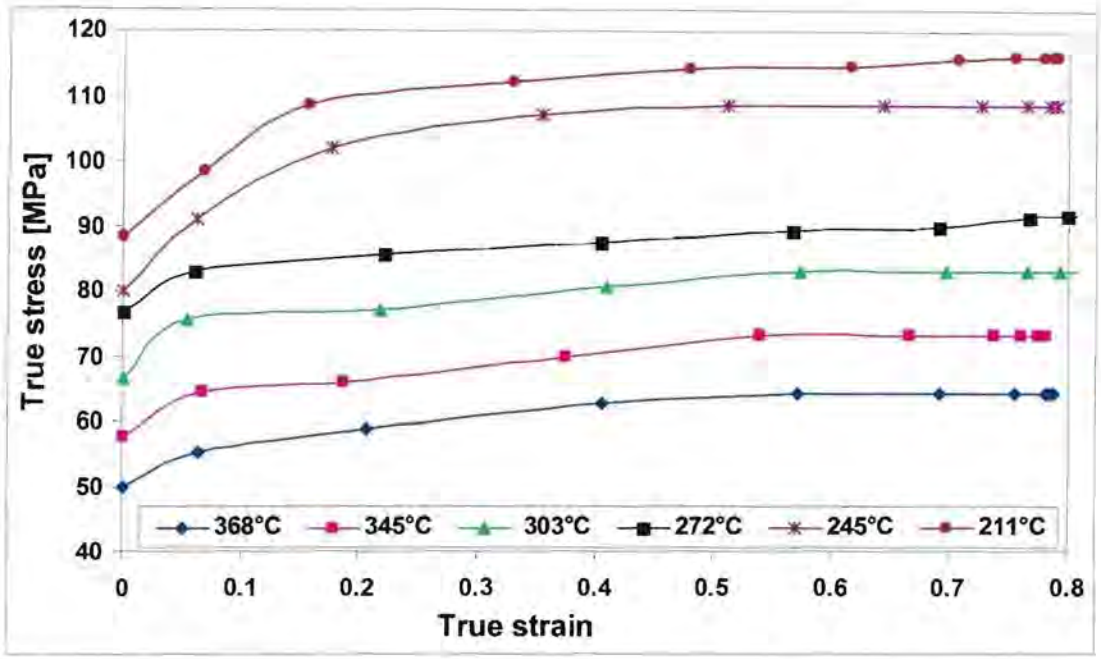

Figure 4-9. PSC flow stress for transfer plate specimens deformed in a temperature range of 211°C to 368°C. ($\varepsilon = 0.8$ and $\dot{\varepsilon} = 10s^{-1}$).

4.2.1 Effects of Deformation Temperature on Microstructure

Figure 4-10 presents microstructures, (a) and (b), of aged PSC specimens deformed at 368°C and 211°C, respectively, which are the two extreme ends of the simulated temperature range shown in Table 4-2 . The micrographs illustrate the variation of grain structure with deformation temperature. The Table 4-2 summarizes the grain size data for the six PSC simulations; the grain sizes were determined on specimens, which had been solution heat-treated at 560°C for 15 minutes, quenched and aged at 175°C for 8 hrs (i.e. as-aged condition).

Figure **4-11** and Figure 4-12 are plots of the grain size as function of deformation temperature and Zener-Hollomon parameter, respectively.

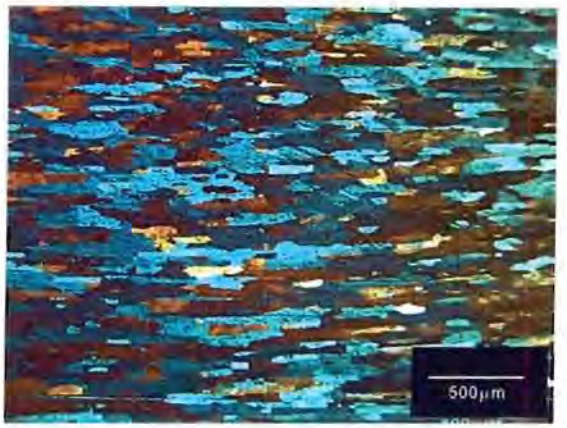

(a) D_T = 37 μm & D_L = 163 μm

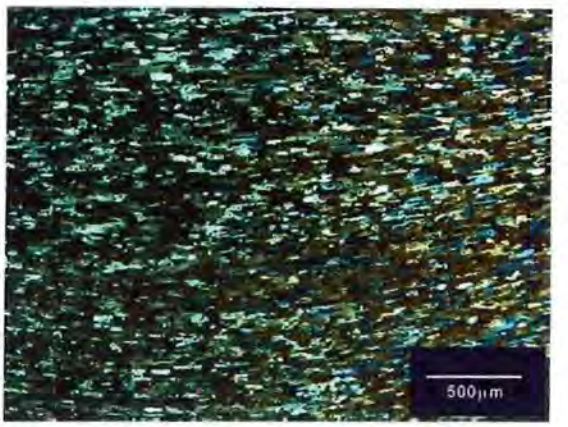

(b) D_T = 20 μm & D_L = 68 μm

Figure 4-10. Microstructures (a) and (b) are from the as-aged PSC specimens deformed at 368°C and 211°C, respectively. (ε = 0.8 and $\dot{\varepsilon}$ = 10s^{-1}).

Specimen No.	PSC temp. T [°C]	Z [s^{-1}]	Grain size D_T [μm]	Grain size D_L [μm]	Aspect ratio D_L/D_T
1	**211**	**2.0E+16**	20	68	3.4
2	**246**	**1.9E+15**	21	72	3.4
3	**271**	**4.2E+14**	25	86	3.5
4	**303**	**7.5E+13**	29	112	3.8
5	**344**	**1.1E+13**	34	146	4.4
6	**368**	**4.0E+12**	37	163	4.6

Table 4-2. Recrystallised grain size data for 1-pass PSC specimens. (ε = 0.8 and $\dot{\varepsilon}$ = 10s^{-1})

A progressive increase in grain size with increase in temperature is observed. The grain size also seems to approach a steady state condition as temperature decreases to below 270°C, **Figure 4-11**. Since Z is also varying with temperature, the grain size is also considered as a function of Z. Z shows a typically opposite effect on grain size to that shown by the temperature, Figure 4-12. The grain size decreases with increase in Z. This is in accordance with the inverse relationship between the temperature and the Zener-Hollomon parameter, Equation 2-3.

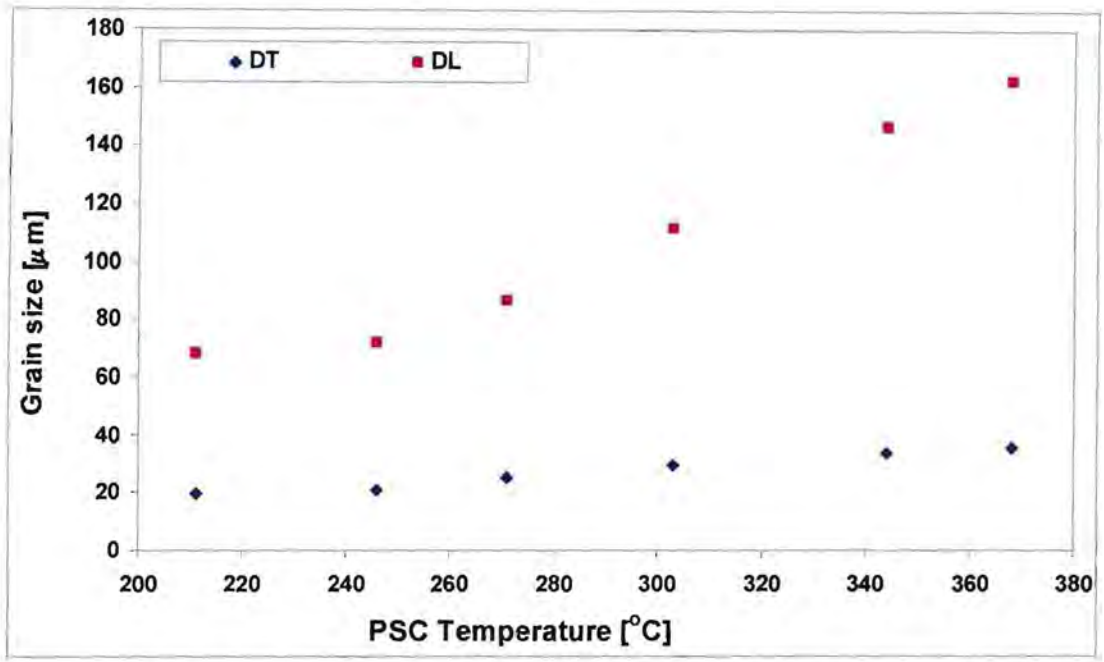

Figure 4-11. Effects of deformation temperature on recrystallised grain size. (ε = 0.8 and $\dot{\varepsilon}$ = 10s^{-1}).

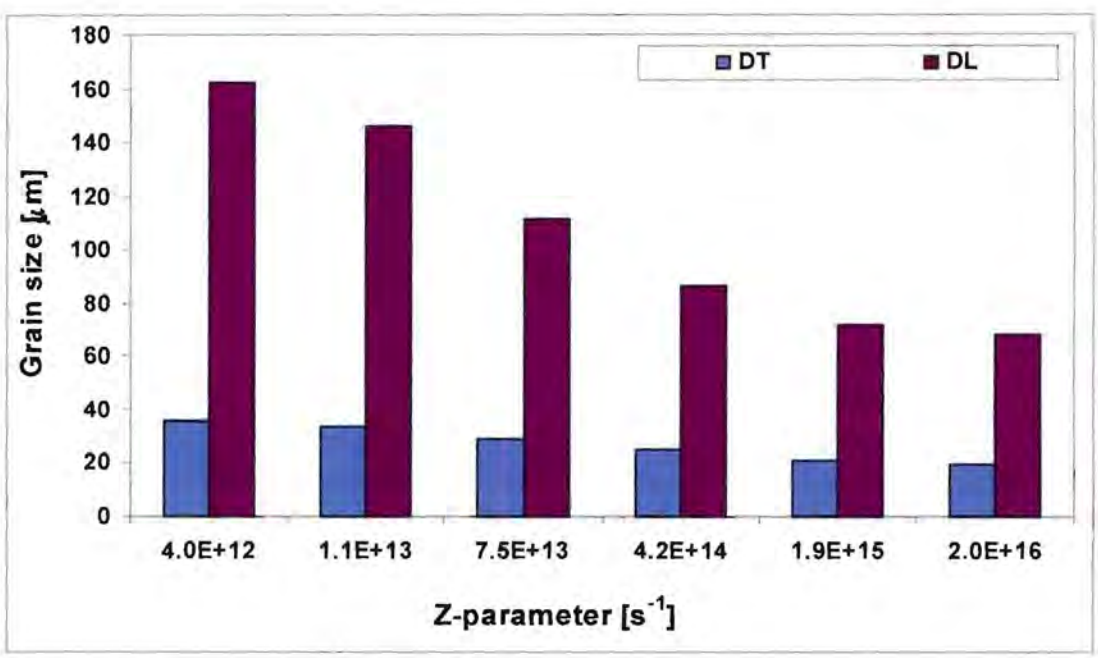

Figure 4-12. Effects of Z on recrystallised grain size. (ε = 0.8 and $\dot{\varepsilon}$ = 10s^{-1}).

Table 4-3 summarizes the recrystallised grain size data and deformation conditions for two-pass PSC simulations. Constant strains (ε_1 = 0.6, ε_2 = 0.3; and ε_T = 0.9) and strain rate ($\dot{\varepsilon}$ = 10s^{-1}) were applied in all the five simulations. (Where: ε_1 and ε_2 are pass1 and pass2 strains, respectively; and ε_T is the cumulative strain = ε_1 + ε_2). Temperature was the controllable variable while inter-pass time and could not be controlled since the rig is air-cooled, however the inter-pass times ranged between just about 2 and 3 minutes, Table 4-3.

Pass1& pass2 temperatures	Inter-pass time	Grain size		Aspect ratio
T_{p1}_T_{p2} [°C]	t [s]	D_T [μm]	D_L [μm]	D_L/ D_T
288_276	122	43	155	3.6
330_291	197	41	169	4.1
340_300	178	43	172	4.0
353_304	184	49	192	3.9
365_317	195	58	252	4.3

Table 4-3. Recrystallised grain size data for 2-pass PSC specimens. (ε_1 = 0.6; ε_2 = 0.3; ε_T = 0.9; and $\dot{\varepsilon}$ = 10s^{-1}).

Just as in 1-pass simulations, the grain size typically increases with deformation temperature. It may also be noted that one-pass simulations generally give finer grain structure compared to the two-pass simulations. This is emphasized by the fact that, even the finest grain size (~ 43 μm) obtained in the two-pass deformations, is larger than the biggest grain size (~37 μm) obtained in single pass simulations. Furthermore, in this particular case, the two-pass deformation temperatures (288°C and 277°C) were much lower than the single-pass temperature (368°C). Furthermore, the total strain for the 2-pass schedule is o.9 while the total strain for 1-pass schedule is 0.8. Therefore, the number of passes involved in the deformation also influences the final grain structure.

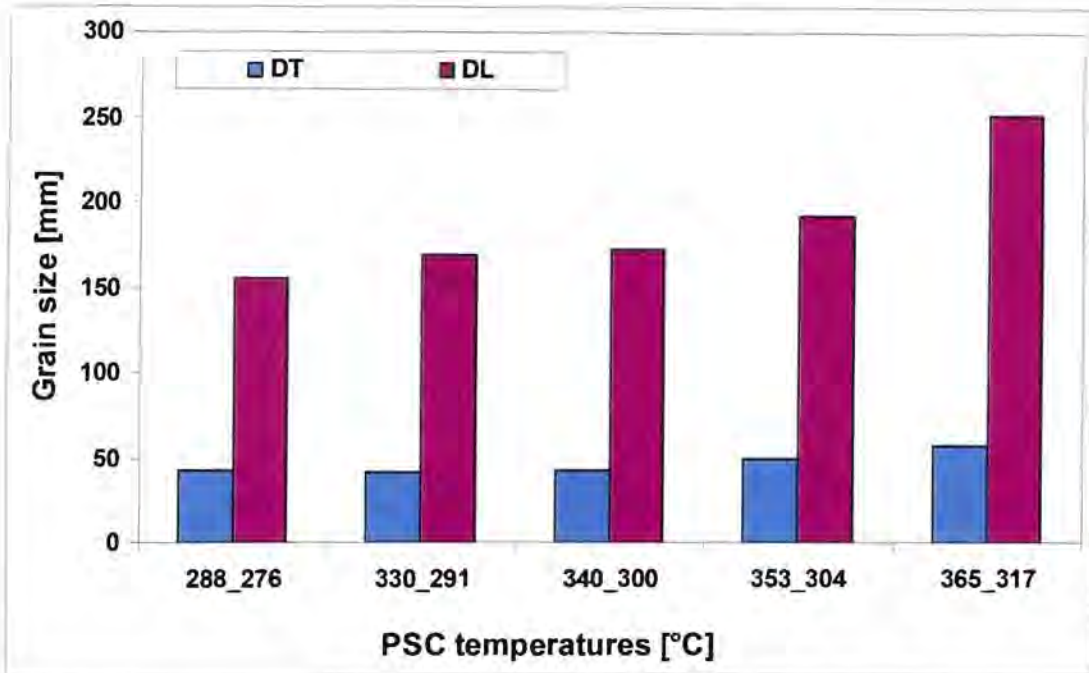

Figure 4-13. Effects of deformation temperatures on recrystallised grain size for 2-pass PSC simulation. (In the x-axis, 1st and 2nd numbers are pass1 and pass2 temperatures used. $\varepsilon_1 = 0.6$; $\varepsilon_2 = 0.3$; $\varepsilon_T = 0.9$; $\dot{\varepsilon} = 10s^{-1}$).

4.2.2 Effects of Deformation Temperature on Mechanical Properties

Hardness tests were done on 1-pass and 2-pass PSC deformed materials, whose deformation temperatures and microstructure grain sizes are given in Table 4-2 and Table 4-3. The hardness was measured in the as-deformed state as well as the heat-treated state. Figure 4-14 and Figure 4-15 are charts of hardness against deformation temperatures for the 1-pass and 2-pass simulations respectively. From the two charts it is observed that for as-deformed material, the hardness decreases with increase in deformation temperature. In single-pass deformations, Figure 4-14, the as-deformed hardness ranges from 65 (for deformation at 211°C), progressively decreasing to 49 (for deformation at 368°C). Similarly, in the two-pass simulations, Figure 4-15, the hardness ranges from 57 (for deformation at 288°C and 276°C) down to 47 (for the specimen deformed at 365°C and 317°C). It

can be inferred that the lower the deformation temperature, the less recovery and hence the higher the dislocation density (or deformation stored energy) in the material. On the other hand, the hardness is observed to be practically similar in all heat-treated specimens, regardless of deformation temperatures or the number of passes used. However, the hardness is much higher than that of the as-deformed state. This, again, shows strengthening to be predominated by solid solution and precipitation, with no manifestation of any grain size influence.

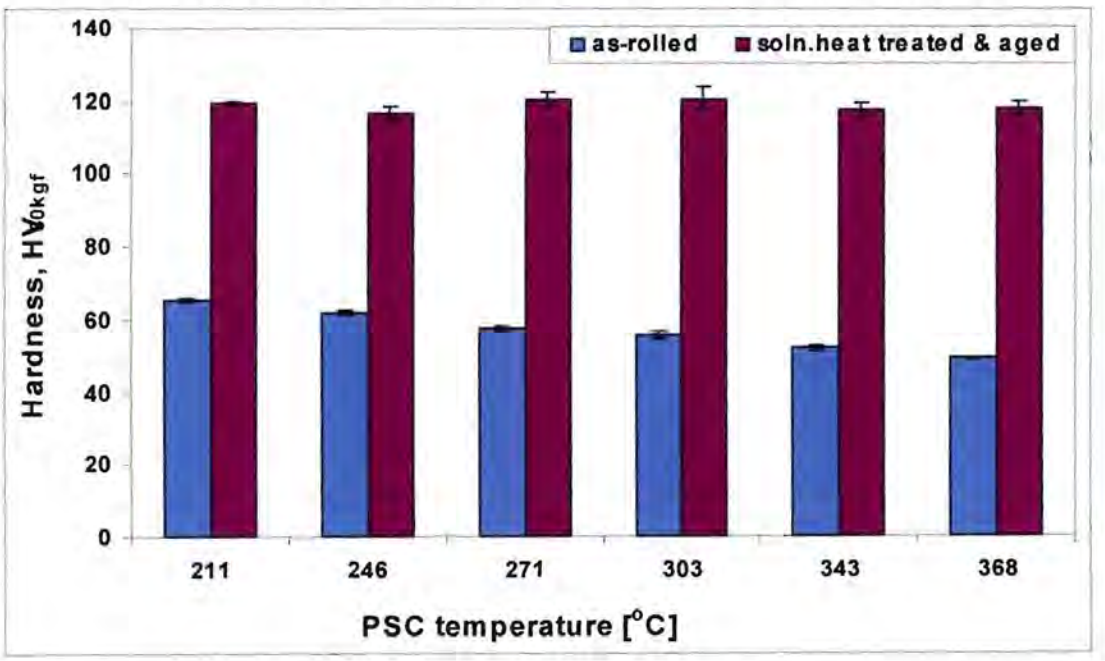

Figure 4-14. Effects of deformation temperature on hardness; in 1-pass PSC specimens. ($\varepsilon = 0.8$ and $\dot{\varepsilon} = 10s^{-1}$).

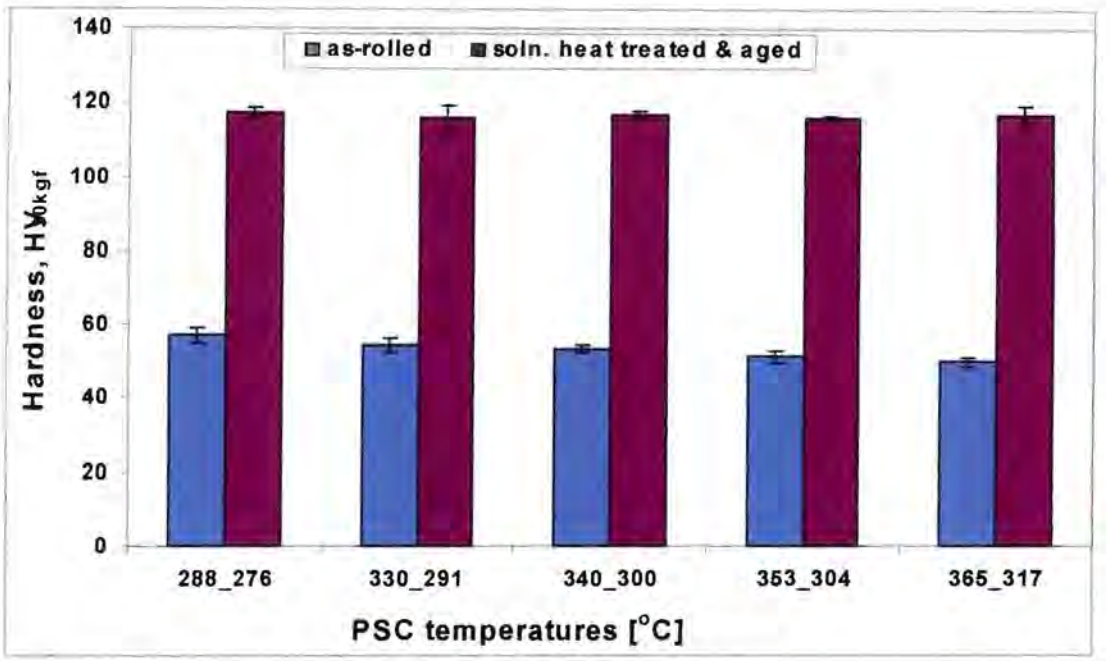

Figure 4-15. Effects of deformation temperatures on hardness in 2-pass PSC specimens. (ε_T = 0.9 and $\dot{\varepsilon}$ = 10s^{-1}).

4.2.3 Effects of Strain on Microstructure and Mechanical Properties

Figure 4-16 shows the effect of varying strain, in the range of 0.2 to 1, on the grain size after ageing. A progressive decrease in grain size as the strain increases is observed. The short-transverse grain size (D_T), for example, decreases from 56 μm in the material deformed to a strain of 0.2, down to 36 μm for the specimen deformed to a strain of 1. However, a steady state condition is reached after a strain of 0.6 as seen by the constant recrystallised grain size from 0.6 onwards. The grain structure remains flat and elongated in the rolling direction with the grain aspect ratio ≥ 4.

Figure 4-17 is a plot of hardness against strain. The material hardness, for both the as-deformed and heat-treated conditions does not exhibit any variation with strain. This is most likely due to the occurrence of intense recovery, which offsets

any strain effects. The deformation temperature of 365°C is significantly high, and therefore would be expected to initiate fast recovery processes. Furthermore, the hardness measuring technique may not be sensitive enough to depict the changes in extent of recovery at each deformation strain.

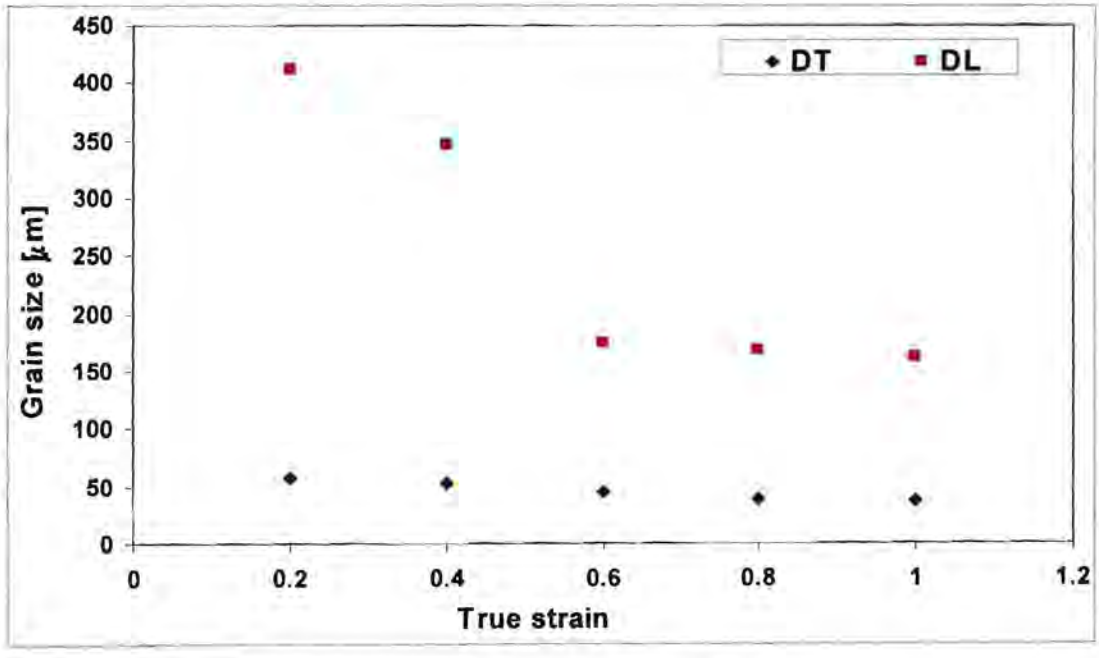

Figure 4-16. Effect of strain on recrystallised grain size. (T = 365°C and $\dot{\varepsilon}$ = 7.5s^{-1}).

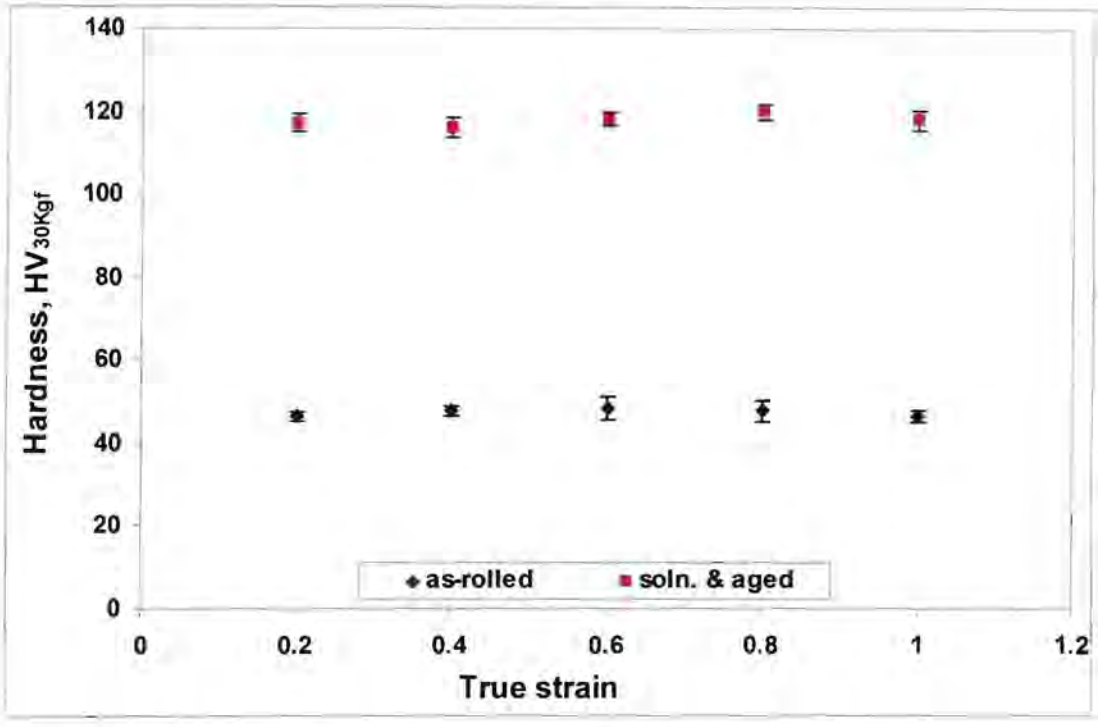

Figure 4-17. Effect of strain on hardness of AA6061 plates. (T = 365°C and $\dot{\varepsilon}$ = 7.5s^{-1}).

4.2.4 Effects of Strain Rate on Recrystallised Grain Size

Figure 4-18 shows the grain size as a function of strain rate at a constant deformation temperature of 365°C and strain of 0.8. It is observed that grain size decreases with increase in strain rate. The grains maintain a typical elongated morphology. The decrease in grain size, as strain rate increases, is typically in line with the grain size behaviour observed in Figure 4-12, where grain size is plotted as a function of the Z. In this case, the Z is concomitantly increasing with increase in strain rate, according to Equation 2-3.

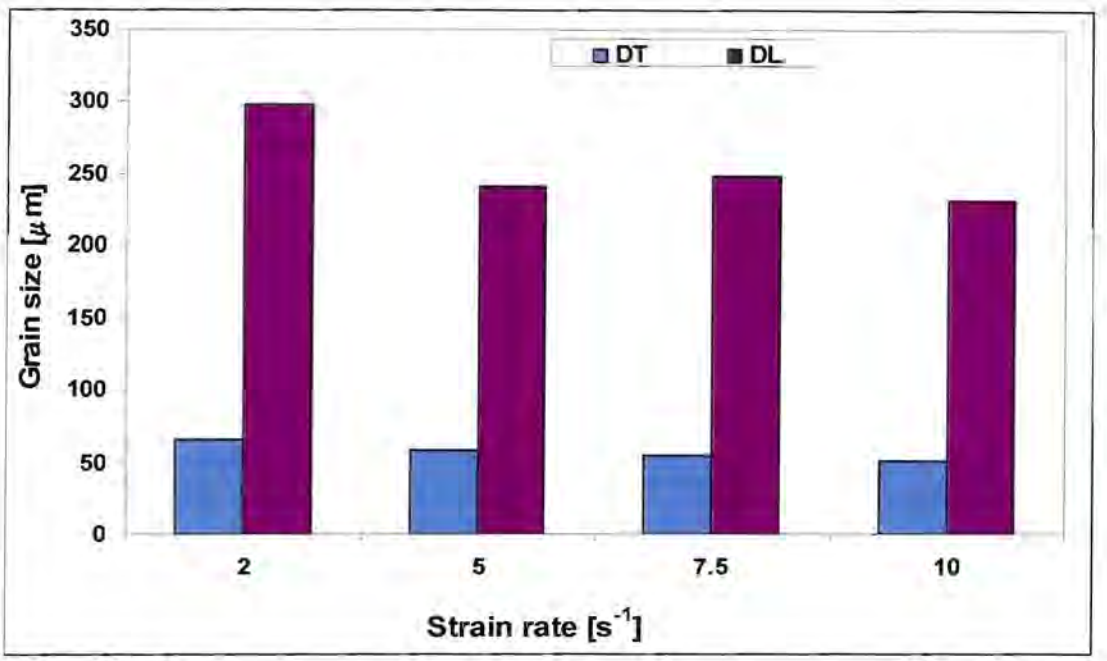

Figure 4-18. Recrystallised grain size as a function of strain rate. (T = 365°C and ε = 0.8).

4.2.5 Effects of Varying Temperature and Strain Rate at Constant Z

Figure 4-19 shows the variation in recrystallised grain size with strain rate and temperature at a constant Z of 7.45E+13s^{-1}. (In the x-axis, the 1st and 2nd numbers are the $\dot{\varepsilon}$ and T used for the PSC test). Strain rates of 2s^{-1} to 10s^{-1} and temperatures ranging 276°C to 303°C were used. A constant strain of 0.8 was applied in the four tests. These tests were specifically to investigate the effect varying temperature and strain rate while keeping Z constant. Although the changes are small, it is observed that the grain size tends to vary with changes in strain rate and temperature though the Z is constant. The grain size increases with increase in both temperature and strain rate. However, grain size has been found to decrease with increase in strain rate, Figure 4-18. Considering the observations

from Figure 4-19 and Figure 4-18 together, it may be inferred that temperature has an over-riding influence on the grain size compared to the strain rate.

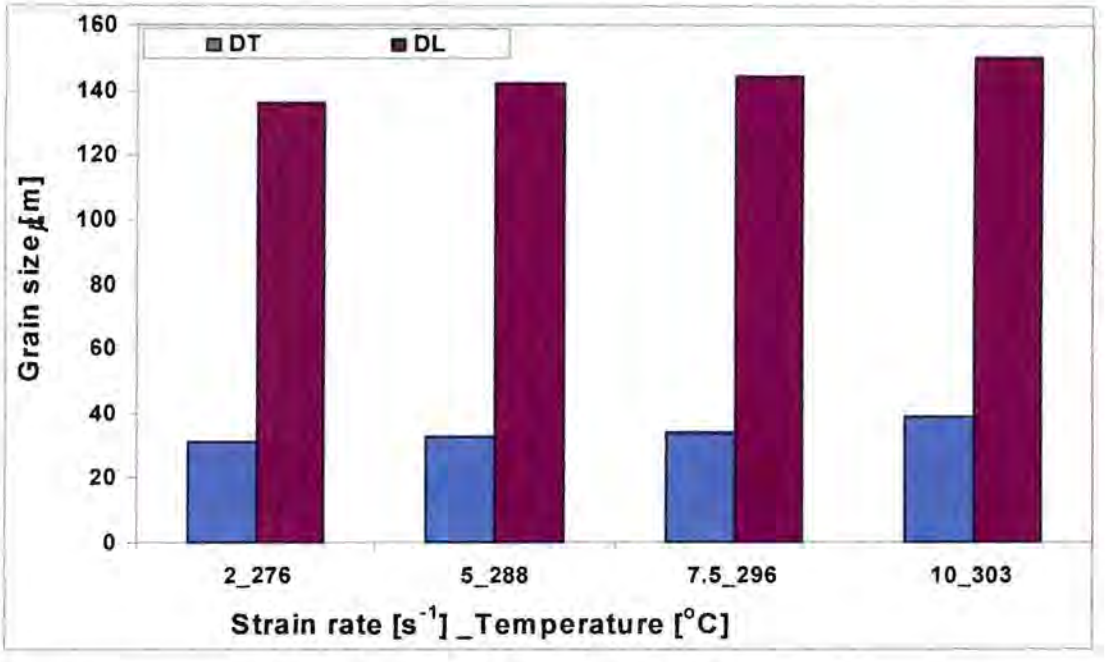

Figure 4-19. Recrystallised grain size as a function of strain rate and temperature at constant Z (= 7.45E+13s^{-1}).

4.3 Finite Element Model Results

The FEM output data of critical interest in this project were the strain and temperature distributions through the plate thickness that were encountered at the rolling instant. Figure 4-20 to Figure 4-23 show some of the FEM output plots of equivalent strain and temperature distribution through the plate thickness for a two-pass simulation. The respective variables are plotted against time. The elements 21, 62, 103, 144 and 185, are the through-thickness elements at the mid-length of the simulated plate (see Figure 3-5), which is where the given variable distribution data were captured. The dashed vertical line in Figure 4-20 and Figure 4-21 is the reference point of interest in the roll-gap.

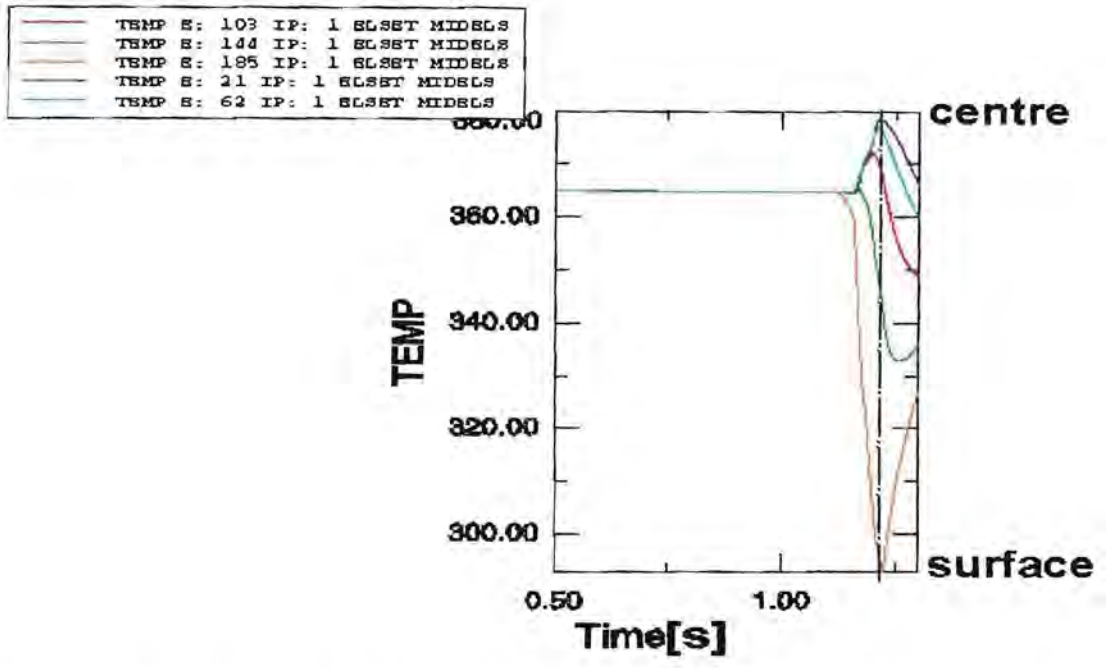

Figure 4-20. Through-thickness T distribution given by FEM for a 1st pass simulation; nominal T= 365°C and nominal ε = 0.62.

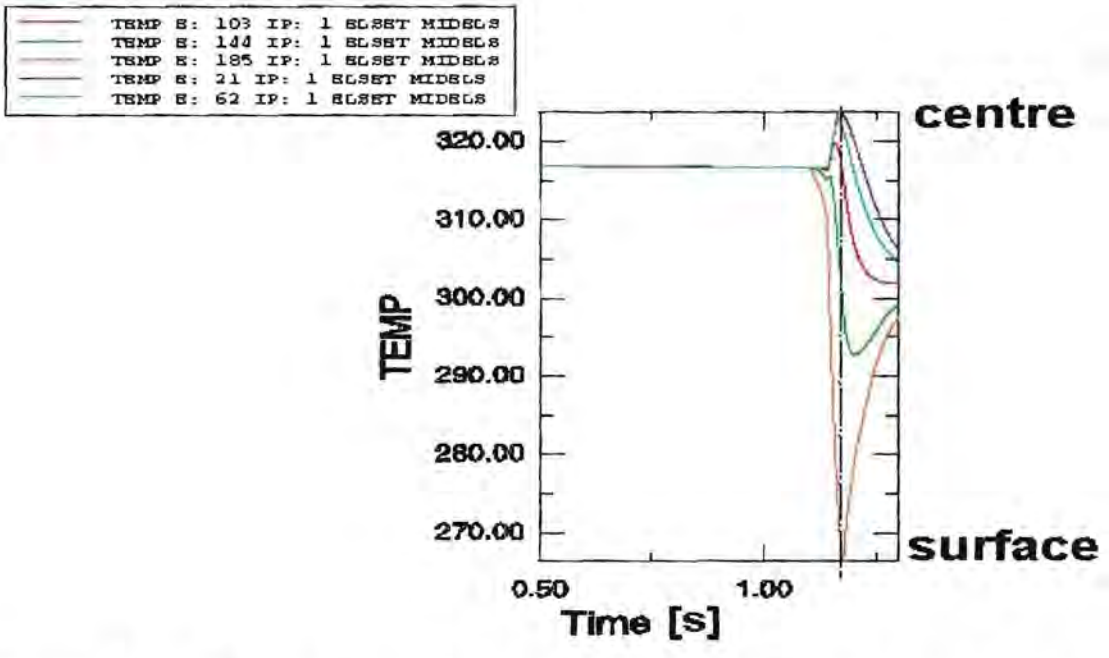

Figure 4-21. Through-thickness T distribution for the 2nd pass simulation; nominal T = 317°C and nominal ε = 0.27.

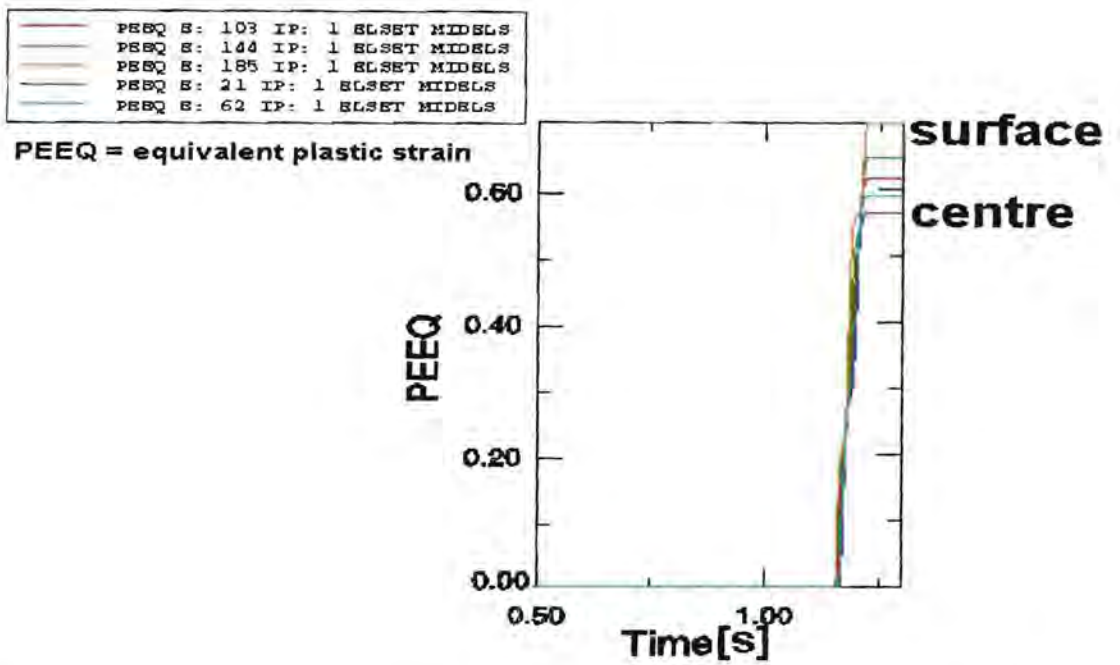

Figure 4-22. Through-thickness strain distribution for the 1st pass simulation; conducted at a nominal ε = 0.62 and nominal T = 365°C.

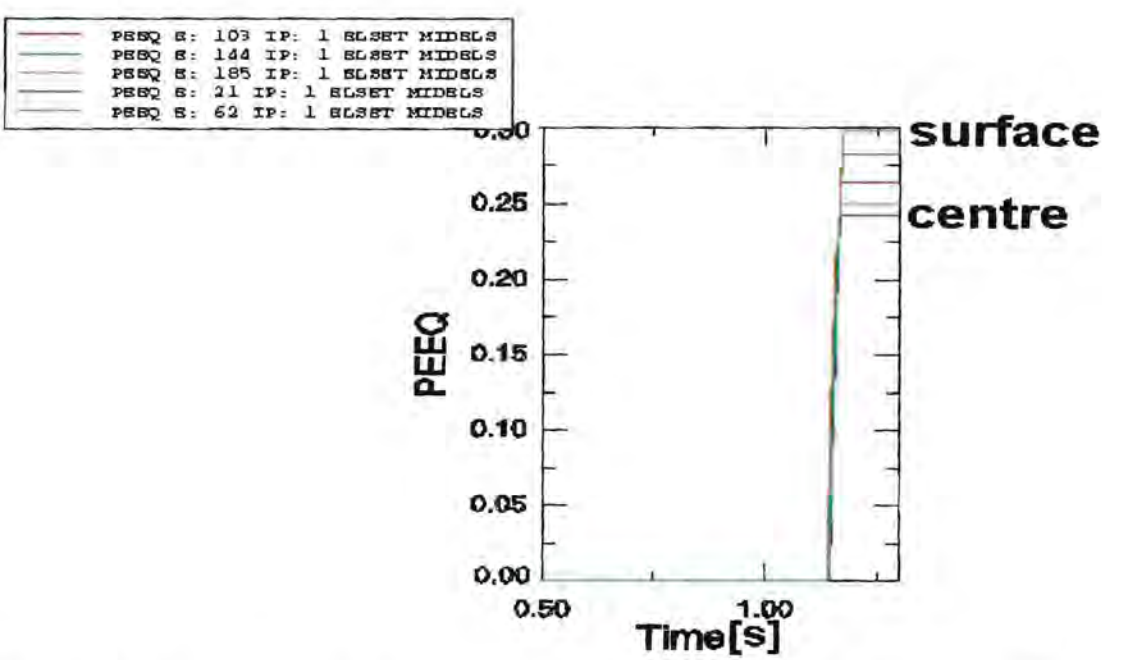

Figure 4-23. Through-thickness strain distribution for the 2nd pass simulation; conducted at nominal ε = 0.27 and nominal T = 317°C.

From the graphs it can be observed that the transient temperatures as well as the accompanying strains are captured. The transient rolling temperatures for the specific elements are read at points where the curves intersect the dotted vertical line. For the equivalent strains the value is read directly on the vertical scale for the respective curves. Figure 4-24 and Figure 4-25 are plots of strain and temperature distributions obtained from the FEM generated plots, Figure 4-20 to Figure 4-23, as function of through-thickness elements. (NB. The 5 elements, 21 (centre) to 185 (surface), in steps of 41, are the centre to surface through-thickness elements at the mid-length point of the simulation mesh (see Figure 3-5)).

Table 4-4 summarizes the FEM-derived variable distributions through the plate thickness. The temperatures and strains are read directly from the plots in Figure 4-20 to Figure 4-23, and the strain rates and Z-parameters are subsequently calculated on the basis of specified FEM input parameters, such as roller speed, roller radius, deformation activation energy and thickness reduction, as well as the temperature and strain outputs from the FEM. Equation 3-2 and Equation 3-3 were applied to calculate the strain rate and the Z-parameter respectively. Also, the deformation activation energy (Q) of AA6061was taken to be **14500JK^{-1}** though out this work.

Element	ε_{p1}	ε_{p2}	ε_T	$\dot{\varepsilon}_{p1}$	$\dot{\varepsilon}_{p2}$	T_{p1}[°C]	T_{p2}[°C]	Z_{p1}	Z_{p2}
21	0.56	0.24	0.80	13	10	378	324	3.1E+12	2.6E+13
61	0.59	0.25	0.84	14	11	376	323	3.5E+12	2.8E+13
103	0.62	0.27	0.89	15	12	372	320	4.3E+12	3.5E+13
144	0.65	0.28	0.93	16	12	350	305	1.2E+13	7.6E+13
185	0.69	0.29	0.98	16	13	295	266	1.7E+14	6.6E+14

Table 4-4. T, ε, $\dot{\varepsilon}$ and Z distributions through plate thickness from FEM.

Figure 4-24 and Figure 4-25 are plots of temperature and strain distributions as function of the mesh elements (or through-thickness positions). It is observed that the FEM predicts maximum temperature at the centre of the work-piece and minimum temperature at the surface. The centre generally registered a slight

increase in temperature relative to the initial temperature of the plate, while the surface showed a significant drop in temperature. On the other hand, FEM predicts maximum strain on the surface, progressively decreasing towards the centre.

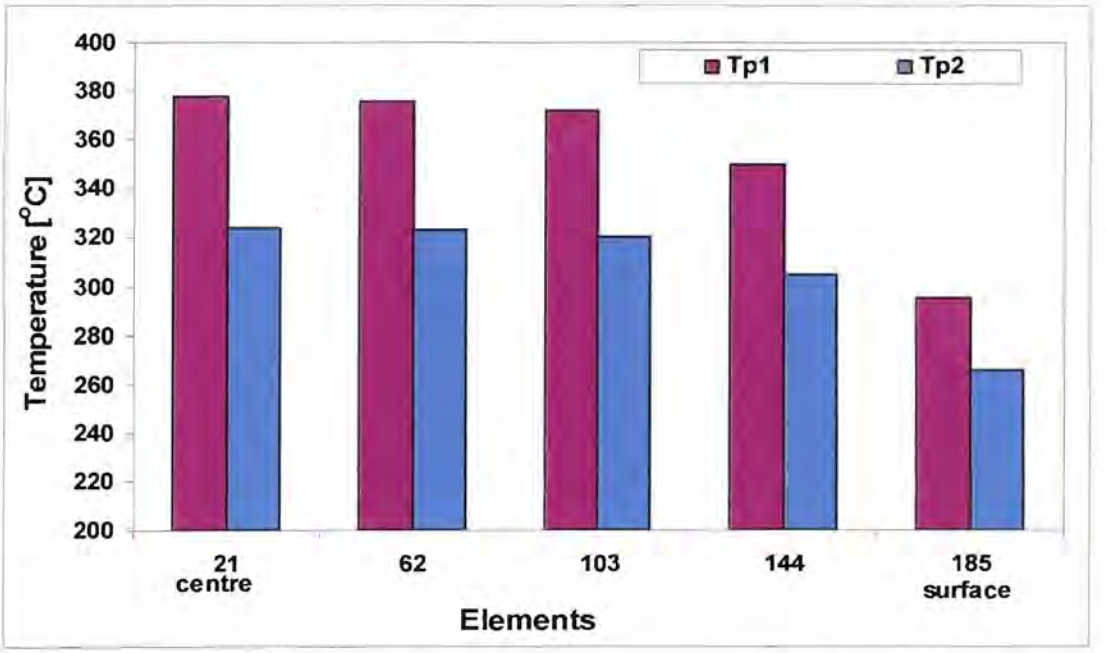

Figure 4-24. Through-thickness T distribution predicted by FEM for 1st and 2nd passes. Nominal temperatures: T_{p1} = 365°C and T_{p2} =317°C.

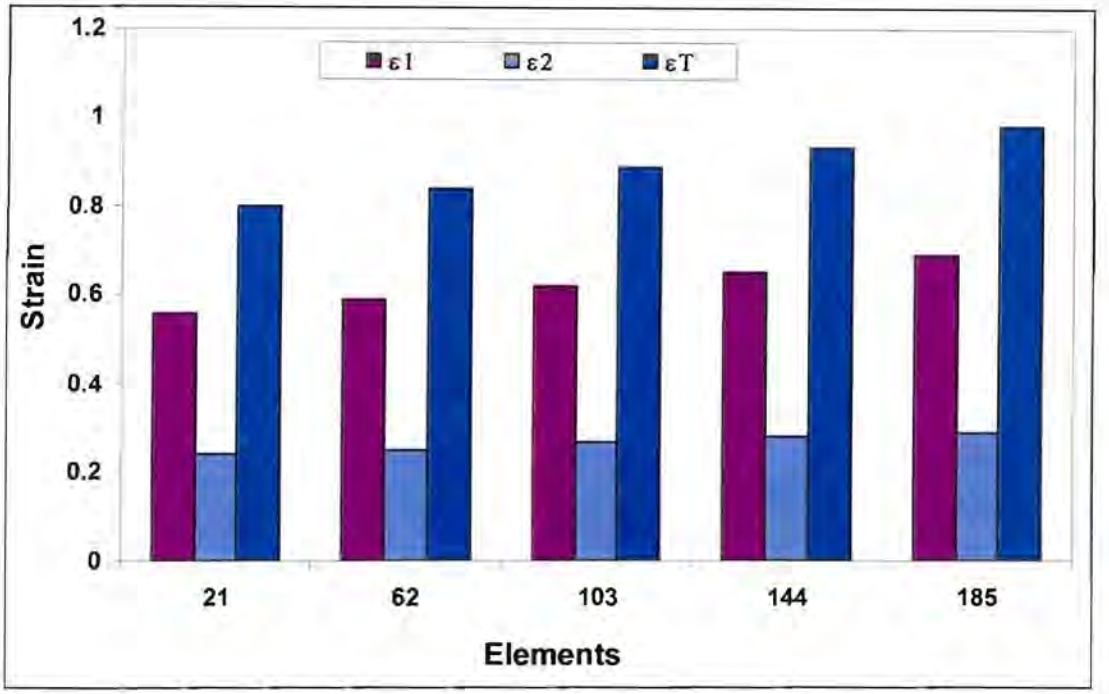

Figure 4-25. Through-thickness strain distribution from FEM. Nominal 1st and 2nd pass strains are $\varepsilon_1 = 0.62$ and $\varepsilon_2 = 0.27$, respectively.

4.4 Two-Pass PSC Testing Based on Actual FEM Predicted Variables

Figure 4-26 shows the recrystallised grain structure as a function of mesh elements (through-thickness position), for two-pass PSC specimens. [The PSC simulation of the individual elements (21 to 185) was achieved by deforming the specimens under strains and Z conditions predicted by the FEM. A strain rate of $7.5s^{-1}$ was applied for both passes in all the five simulations; however, temperatures were altered such that the respective Z parameters, given in Table 4-4, were maintained.] As expected, the grain size increases from the surface (D_T = 20 μm) to the centre (D_T = 50 μm). This grain size trend could easily be inferred by just considering the FEM predicted variable distributions, Table 4-4, and the effects of these individual parameters on the grain size structure, which have already been

investigated quite extensively elsewhere in this project. The grains also exhibit a flat and elongated morphology.

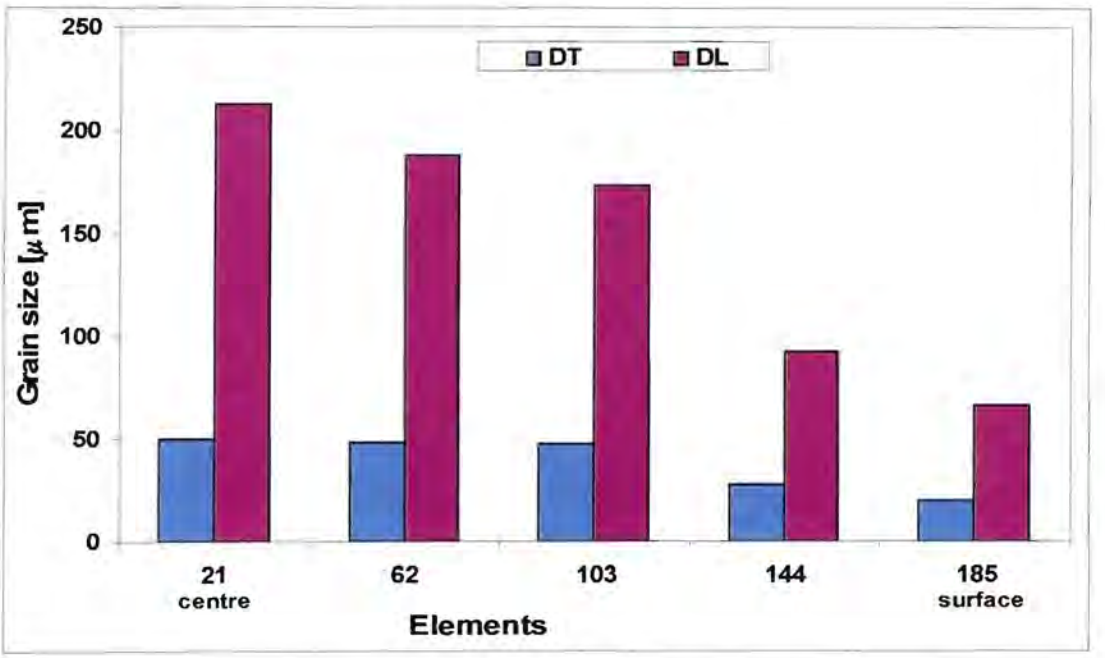

Figure 4-26. Through-thickness recrystallised grain size from 2-pass PSC specimens; each element was simulated using T and ε predicted by FEM.

Chapter 5

5 DISCUSSION

5.1 Characterisation of As-Received Plates

5.1.1 Microstructure

The optical micrographs of as-rolled specimens, from transfer and finished plates, Figure 4-1, show microstructures consisting of continuous deformed bands, parallel to the rolling direction (RD). The deformed structures do not reveal any significant grain size information. Metallographic pictures from heat-treated transfer and finished plates, Figure 4-2 and Figure 4-3, respectively, show fully recrystallised structures. The recrystallised microstructures have flat and elongated grain morphologies, with grains are typically elongated in the rolling direction. The elongated grain morphology is most likely due to the anisotropy in particle shape, orientation and distribution, through the plate thickness. The distribution, shape and orientation of particles have profound influence on the degree and the mode of their pinning effect[4,20]. For instance, during the thermomechanical processing, particles are strung in the working direction (a process called *mechanical-fibering*). Consequently, the particles will have a rod or plate-like shape aligned parallel to RD; this helps to sustain the elongated or "pancake"-shaped grains developed during working. The particles also tend to possess a longer mean free path in the RD than the ND, and as a result there is more opposition to grain boundary mobility in the ND than in the RD. Therefore, grains grow faster in the RD[4]. Also, uneven distribution of particles is quite common in many alloys, and situations in which particles are concentrated in planar bands are often encountered in rolled products. This makes it difficult for grain boundaries to migrate through such bands and expand in the direction perpendicular to those bands; as a result grain growth is restricted to the directions parallel to the bands[20].

The transfer (26 mm thick) plate, Figure 4-2, does not exhibit significant variation in through-thickness grain structure. The grain structure could safely be regarded as uniform from the surface to the centre. However, the transfer plate shows a coarser grain structure (overall mean D_T = 76 μm) as compared to the finished plate, (overall mean D_T = 60 μm, for industrial heat treated specimens)

The finished plate microstructure shows a through-thickness grain size gradient, with grain size being largest at the surface and progressively decreasing towards the centre. The mean short-transverse grain size for the surface structure was determined to be approximately 1.3 times that of the centre structure. There are numerous possible metallurgical and/or mechanical processing factors that may be responsible for these grain size gradients in the material. Among them are, inhomogeneities in dislocation density (or stored energy) and second phase particle distribution effect. The pinning effect of particles has already been elucidated above; suffice to say grains are likely to be finer in regions with a higher concentration of particles, when the overall particle distribution is uneven. The uneven distribution of particles, among other things, tends to exacerbate the deformation inhomogeneities, which in turn may cause disparities in the stored energy within the deformed material. This usually results in microstructure evolving differently within the same material.

5.1.2 Through-thickness Particle Distribution

An investigation of the particle distribution through the plate thickness by optical microscopy, Figure 4-7 and Figure 4-8, did not reveal any particle distribution gradients. However, these results, on their own, cannot be considered adequately conclusive. The distribution gradients may be present on such a finer scale, which could not be detected by optical microscopy. A further check using other techniques that are capable of offering better resolution might allow more conclusive deductions to be made. However, hardness measurements through the thickness of the plates, as discussed in detail hereafter, section 5.1.3, do not

suggest any particle distribution gradients either. Typically, finer structure - as observed at the centre of the finished plate - would imply a higher concentration of particles in that region of the plate. As such, higher hardness values would be expected in that region, especially in a material that derives its strength from precipitation and solid solution hardening, as AA6061.

5.1.3 Hardness

Through-thickness hardness profiles of the transfer and finished plates are depicted in Figure 4-4 to Figure 4-6. The materials were tested in three different conditions, namely, (a) as-deformed, (b) solution heat-treated and (c) solution heat-treated and aged. The as-deformed hardness, for both the transfer and finished plates, do not show any significant variation through the thickness of the individual plates. Actually, the hardness values are virtually the same through the plate thickness. The overall average hardness values are 48 ± 2, for the transfer plate, and 52 ± 2, for the finished plate. This suggests absence of stored energy and particle distribution gradients through the plate thickness or implies that the hardness test technique, in this case, may not have been sensitive enough to detect such inhomogeneities. The uniform through-thickness hardness further suggests that the grain size gradients, observed in the finished plate (Figure 4-3), may not necessarily be due to stored energy differential through the plate. Therefore, other metallurgical and/or thermomechanical phenomena could be responsible for the grain structure inhomogeneity.

Comparison of the as-deformed hardness profiles, Figure 4-6, reveals that the finished plate gives slightly higher hardness than the transfer plate. This meets with the expected increase in dislocation density of finished plate, resulting from the additional strain, in the HFM stage, where it is reduced from 26 mm to 13 mm thick and perhaps more importantly, the lower deformation temperature of the finished plate. The slight difference in the as-deformed hardness between the two plates logically explains the observed difference in their recrystallised grain sizes.

Generally, in the heat-treated conditions, some slight through-thickness variations in hardness of individual plates are observed, Figure 4-4 to Figure 4-6. Notably, the through-thickness hardness profiles show minima at the mid-thickness of the specimens. The phenomenon appears to be more pronounced in those specimens tested after solution heat treatment only, and less so in those specimens that have been subjected to solution heat treatment plus ageing. The fact that the hardness values exhibit some through-thickness variations in solution heat-treated specimens only, and not so in the as-deformed specimens, seems to rule out stored energy and particle distribution patterns as possible causes of these through-thickness hardness variations. Grain size effect cannot reasonably explain these variations either, since lowest hardness values are recorded at the centre, even in the finished plate specimens, where grain structure is actually finer in that region. Furthermore, if the phenomenon was due to grain size variation within the plate then ideally similar or even more pronounced hardness variation between the transfer and finished plates would have been exhibited, since grain size between the two plates is even larger than that observed within a the individual plate. In fact, the hardness profiles for the finished and transfer plates are more or less a duplicate of each other, Figure 4-6, for similar heat treatment conditions. These observations seem to suggest the residual stress effect as the main cause of the through-thickness hardness variations in heat-treated specimens. Significant residual stresses are quite likely to be present in the specimens as a result of the rapid cooling, due to water quench, from the solution heat treatment temperature of 560°C to room temperature. Also, the fact that the variation is found to be more prominent in those specimens that have been subjected to solution heat treatment plus quenching only compared to those that have undergone a full heat treatment cycle, supports the idea of residual stress effect. The ageing process is well known for its role in relieving residual stresses induced during quenching and/or any other prior processes. This explains why the variations in hardness are apparently in those specimens subjected to the ageing process subsequent to the quenching.

There are no significant differences in magnitude between the hardness values of heat treated transfer and finished plates, despite the notable differences in grain size. In fact, the hardness profiles for the heat-treated finished and transfer plates are more or less duplicates of each other, Figure 4-7. This clearly indicates that the grain size effect is not the major strengthening mechanism in AA6061 material; especially in the investigated grain size regime. Precipitate hardening and solute hardening are presumably the predominant mechanisms. This notion is supported by the material's positive response to heat treatments. The material hardness, typically, increases with solution heat treatment and ageing processes, confirming precipitation and solid solution hardening as the predominant strengthening mechanisms.

Grain size may not have a significant effect on the mechanical strength of aluminium alloys, or at least in AA6061 especially, as inferred from the similarities in hardness profiles of plates with significantly different grain size. However, grain size is also known to influence a host of other material properties, such as creep resistance, corrosion and surface roughening. Therefore, grain size control, even in an alloy where it does not seem to influence the strength, remains a critical issue. Therefore, the microstructural and mechanical response of AA6061 to thermomechanical processing still warrants intense investigation.

5.2 Effects of Thermomechanical Variables on Grain Size and Hardness

5.2.1 Effects of Deformation Temperature on Grain Size

Metallographic analyses of annealed (solution treated) 1-pass and 2-pass PSC specimens show that grain size decreases with decreasing deformation temperature, as shown in Figure 4-11 and Figure 4-13. The grain size refinement,

however, tends to approach a steady state condition as the deformation temperature decreases to below 270°C. Also, comparison of recrystallised grain size of specimens deformed by 1-pass and 2-pass schedules reveals that single pass deformations tend to give finer grain structures than two pass deformations – that is for the similar overall strains and strain rates. This is clearly evident when considering that the finest grain size (~ 43 μm) obtained in the two-pass simulations, at deformation temperatures of 288°C and 277°C, is even larger than the biggest grain size (37 μm) obtained in single pass simulations, when a much higher deformation temperature of 368°C was used. The coarser grain structure, that results from the multi-pass deformation process, could be due to the fact that the specimens are held in contact with hot platens for an extended period (inter-pass time), as the system awaits the pre-set conditions of the succeeding pass to be attained. During the inter-pass time significant recovery occurs since the operating temperatures are relatively high. This results in a deformed structure with larger subgrain size compared to the 1-pass deformed structure. Consequently the recrystallised grain structure that evolves is expected to be larger in the 2-pass than in 1-pass deformation specimens.

On the basis of these results, it may be inferred that grain refinement can be achieved in AA6061 by lowering deformation temperatures as well as minimising the number of deformation passes, particularly in the HFM – of course, this implies larger deformation loads and higher strains per pass.

In a situation where temperature is varied and strain rate is kept constant, then Z varies concomitantly with temperature, and in this case the grain size can also be considered as a function of Z. The grain size decreases with increase in the value of Z, Figure 4-12. Thus the effect of Z on the grain size is typically opposite to that of temperature, which is well in accordance with the inverse relationship between Z and T, Equation 2-3.

5.2.2 Effects of Temperature on Hardness

For the as-deformed condition, in both 1-pass and 2-pass specimens, hardness decreases with increase in deformation temperature. For example, hardness values for the 1-pass deformed specimens ranges from 65, for a specimen deformed at 211°C, and progressively decreases to 49, for a specimen deformation temperature of 368°C, Figure 4-14. The observed trend is due to faster recovery processes at the higher deformation temperatures. On the other hand, lower deformation temperatures result in dislocation build-up due to slow recovery and hence higher hardness due to more retained deformation energy.

In the solution heat-treated condition, hardness is found be practically similar for all the specimens, irrespective of deformation temperatures or the number of passes and despite grain size differences. This further confirms that grain size does not significantly influence the strength of this alloy. Again, this leaves precipitation hardening and solid solution hardening, as the only key strengthening mechanisms.

5.2.3 Effects of Strain on Microstructure and Hardness

Investigation into the effects of strain on microstructure and mechanical properties of AA6061 was conducted by deforming a series of specimens in a strain range 0.2 to 1; at 365°C and $10s^{-1}$. The recrystallised grain size progressively decreases as the strain increases from 0.2 to 1, Figure 4-16. For instance, the short-transverse grain sizes (D_T) of the specimens deformed at the two extremes of the strain range were measured to be 56 μm (for $\varepsilon = 0.2$) and 36 μm (for $\varepsilon = 1$). However, a steady state condition is reached after a strain of 0.6 as seen by the constant recrystallised grain size from 0.6 onwards, Figure 4-16. The grain morphology remained largely flat and elongated in the rolling direction, with the grain aspect ratio ≥ 4.

The hardness, in both as-deformed and heat-treated specimens, did not exhibit any variation with strain, Figure 4-17. The fact that strain variation did not result in hardness variation in the as-deformed specimens suggests the recovery process were high enough to annihilate most of the deformation energy. It is quite rational to expect a significantly high degree of the restoration mechanisms when an aluminium alloy, such as AA6061, is deformed at a high homologous temperature, such as 365°C. Furthermore, the hardness measuring technique may not be sensitive enough to depict the changes in extent of recovery at each deformation strain. Again, no grain size effect on the hardness is manifested since the annealed specimens do not show significant variation in hardness. The hardness however, increases with heat-treatment showing solid solution and precipitation strengthening effects, Figure 4-17.

5.2.4 Effects of Strain Rate on Recrystallised Grain Size

A range of strain rates, $2s^{-1}$ to $10s^{-1}$, was used to investigate the effects of strain rate on the grain structure of AA6061. A strain of 0.8 and temperature of 365°C was used. The grain size decreases with increase in strain rate, Figure 4-18. However, the grains maintain an elongated morphology, with a grain aspect ratio of ~ 5. Again, it is interesting to note that, in this case, Z is also concomitantly increasing with increase in strain rate, according to Equation 2-3. These results are therefore typically in line with the behaviour observed when the grain size was considered as a function of Z, Figure 4-12.

5.2.5 Effects of Varying Temperature and Strain Rate (Constant Z)

As discussed in sections 5.2.1 and 5.2.4, temperature and strain rate have a counter effect on the grain size. Since Z is a function of temperature and strain rate, Equation 2-3, it was deemed necessary to have a check on what happens to

dropped significantly, relative to the initial (nominal) temperatures of the plate, presumably due to the roll chilling effect. The interior parts, particularly the centre, registered slight increases in the temperatures, presumably due to adiabatic heating being high enough to offset the heat losses. For example, in a plate with an initial temperature of 365°C, the temperature of the surface was predicted to be 295°C, which is about 19% drop, while that of the centre registered as 378°C, that is approximately 4% increase (Figure 4-20 and Figure 4-21). The model results were applied in the subsequent PSC simulation of some selected industrial rolling schedules. The predicted strain distribution trend, on the other hand, was the reverse of the temperature distribution trend. The Z and $\dot{\varepsilon}$, were derived from the FEM outputs, and both showed increasing trends from centre to surface, Table 4-4.

The through-thickness temperature and strain distribution trends predicted by the FEM are qualitatively in line with what other researchers have observed, albeit working with different materials and conditions[40]. The model outputs were then applied in PSC to simulation of a few selected rolling schedules in order to verify how the variable distributions influence the through-thickness grain structure.

5.3.1 Through-thickness Grain Structure Evolution by PSC and FEM.

The PSC simulation, of the conditions experienced by individual elements through the plate thickness, was achieved by deforming a series of specimens at the strains and Z conditions predicted by the FEM, Table 4-4. A uniform strain rate of $7.5s^{-1}$ was applied in all these simulations. However, temperatures were adjusted such that the respective Z values, as given in Table 4-4, were maintained. The through-thickness regimes (elements) had to be simulated on the basis of Z, rather than the actual predicted strain rates and temperatures, because the predicted strain rates were much higher than the stipulated maximum limit ($10s^{-1}$) of the rig. As expected, the grain size increases from the surface (D_T = 20 μm) to the centre

(D_T = 50 μm), Figure 4-26. The grain size trend could be readily inferred by just considering the FEM predicted variable distributions, Table 4-4, and the effects of these individual parameters on the grain size structure, which have already been discussed quite extensively, in the preceding sections. The grains, generally exhibit a flat and elongated structure, with aspect ratios ≥ 3.

Chapter 6

6 CONCLUSIONS

This work has extensively explored the qualitative and quantitative effects of the three critical thermomechanical variables – temperature, strain and strain rate – on the grain structure and hardness of AA6061. On the basis of these investigations the following key conclusions can be drawn:

- Grain size is sensitive to thermomechanical variables – temperature, strain and strain rate.

- Grain refinement can be achieved by deforming at relatively low temperatures, high strains, and high strain rates.

- Grain size has no significant influence on the material strength in heat-treated AA6061 alloy. The strengthening is predominantly by solid solution and precipitation hardening.

- FEM predicts that during hot rolling the temperature is lowest at the surface and maximum at the centre of the work-piece, while strain, strain rate and the Zener-Hollomon parameter are highest at the surface and lowest at the centre of the work-piece.

- On the basis of the FEM temperature, strain and strain rate distributions, the final plate should always have a finer grain structure on the surface relative to the grain size at the centre.

- There was no evidence, therefore, that the coarser surface grain structure observed in some commercial finished plates, could be attributable to any

one or combination of the investigated deformation variables – temperature, strain and strain rate. Other factors could be responsible for this inconsistent grain size trend.

- No definitive through-thickness particle distribution patterns are observed by optical microscopy. It is not possible, however, to conclusively rule out the presence of such particle concentration gradients through the plate thickness, which might probably help to explain the grain size trends.

Chapter 7

7 RECOMMENDATIONS

Based on the conclusions, particularly the fact that the question of through-thickness grain-size gradients remains unresolved, the following recommendations are made:

- The question of whether or not particle distribution patterns are responsible for the observed through-thickness grain-size gradients in some commercial plates warrants further investigation. Conclusive deductions may possibly be achieved by conducting further metallographic analyses on the plates. This may entail application of more sophisticated techniques, such electron microscopy. Further optical microscopy may also be considered, particularly at higher magnification levels, say 1 500X. At 1 500X magnification, features as small as 0.1 μm can be resolved, and second-phase particles, of sizes ≥ 1 μm, can be clearly identified[1].

- Tribological parameters, especially *friction*, encountered during hot rolling also need to be investigated. Friction, usually defined by the coefficient of friction, depends on a large number of variables, which makes it a rather complex parameter. Some of the factors, which influence friction are: roughness and hardness of the interacting surfaces, yield strength, strain hardening coefficient, amount of reduction per pass, temperature, velocity and lubricant viscosity. Lenard et al[50] highlighted that the traditional Coulomb friction model, generally applied in modelling most forming processes, and was also applied in this particular study, does not adequately capture the friction conditions encountered in real forming processes. Possible improvements on the friction modelling need to be considered since friction impacts on the strain and temperature distribution

through the work-piece. In addition, investigation of the influence of friction on microstructural evolution is also suggested.

8 REFERENCES

1. Hatch, J.E. (ed.), ***"Aluminium: Properties and Physical Metallurgy"***, ASM, Park, Ohio, 2nd edition (1988).
2. ASM Handbook, ***"Properties and Selection: Non-Ferrous and Special- Purpose Materials"***, Vol. 2.
3. Polmear, I.J., ***"Light Alloys: Metallurgy of the light metals",*** Metallurgy and Materials Science Series, Ed. Honeycombe, R.W.K. and Hancock, P.
4. Starke, A., Jr., ***"Heat Treatable Aluminium Alloys",*** Aluminium Alloys Contemporary Research and Applications, Ed. Vasudevan, A.K. and Doherty, R.D.
5. Doward R.C., Bouvier C., ***"A rationalization of factors affecting strength, ductility and toughness of AA6061-type Al-Mg-Si-(Cu) alloys"***, Material Science and Engineering A254, (1998) pp 33- 44.
6. Lillywhite S. J., Prangnell P.B., Humphreys J., ***"Interactions between precipitation and recrystallisation in an Al-Mg-Si alloy"***, Materials Science and Technology, **Vol.16** (2000) pp 1112-1120.
7. Zhuang I., Bottema J., Kaasenbrood P., Miller W.S., and de Smet P., ***"The effect of small particles on annealed grain size and texture of Al-Mg-Si alloys"***, Material Science Forum, **Vol.217-222** (1996) pp 487-492.
8. Singh R.K. and Singh A.K., ***"Evolution of Texture during Thermo-Mechanical Processing of an Al-Mg-Si-Cu Alloy"***, Scripta Materialia, **Vol.38**, 8 (1998) pp1299-1306.
9. L. Polmear, ***"Microstructures and strengthening of aluminium alloys",*** Deformation of Polycrystals: Mechanisms and Microstructures, Ed. Hansen N., Horsewell A., Leffers T. and Lilholt H., 2nd Riso Int. Symp. On Metallurgy and Materials Science, pp 99-110, 1981.

10. Embury, J.D., Lloyd, D.J. and Ramachandran, T.R., ***"Strengthening Mechanisms in Aluminium Alloys",*** Ed: Vasudevan, A.K. and Doherty, R.D.,Treatise on Mat. Sci., and Technology, **Vol. 31**, p 579-601 (1989).
11. Hall, E.O., Proc. Phys. Soc., London, **B64**, 747 (1951).
12. Carreker, R.P., and Hibbard, W.R., Met. Trans. A.I.M.E., **209**, 1157 (1957).
13. Phillips, V.A., J.I.M., **81**, 623 (1952).
14. Fleischer, R.L., Acta Met., **11**, 203 (1963).
15. Nobel, F.W., Harris, S,J. and Dinsdale, K., Met. Soc., **16**, 425 (1983)
16. King F., ***"Aluminium and its alloys",*** Ellis Howard Limited (1987).
17. Beddoes J. and Bibby M. J., ***"Principles of Metal Manufacturing Process",*** John Wiley and Sons Inc., New York.
18. Carmel, L. J., King, F. and Salt, G., ***"Hot Rolling of Sheet and Strip: Aluminium and Aluminium Alloys",*** Metals Tech., August 1975, p 313
19. Hirch J., ***"Thermomechanical Processes in Hot of Rolling of Aluminium"***, Proc. of Int. Conf on thermomechanical processing in theory, modelling and practice (1996).
20. Humphreys F. J. and Hartherly **"Recrystallisation and Related Annealing Phenomena"**, Pergamon.
21. Porter, D.A., Easterling, K.E., **"Phase Transformation in Metals and Alloys"**, Van Nostrad Rheinhold (UK) Co.Ltd., 1981
22. Blum W. and McQueen H. J., ***"Dynamics of Recovery and Recrystallisation",*** Materials Forum **Vols. 217-222** (1996) pp 31-42.
23. Schaller, R. and Riivire, A. ***"Recrystallisation",*** Mechanical Spectroscopy (2001) pp 276-290
24. Rowe G. W., **"Principles of metal working processes"**, Edward Arnold (Publishers) Ltd., (1977) p 208.
25. Duly D., Baxter G. J., Shercliff H. R., Whiteman J. A., Sellars C.M and Ashby M.F. ***"Microstructure and Local Crystallographic Evolution in an Al-1wt% Mg Alloy Deformed at Intermediate Temperature and High Strain-Rate",*** Acta Met., **Vol. 44**, No. 7 (1996) pp 2947-2962.

26. Siwecki T. ***"Modelling of Microstructure Evolution During Recrystallization Controlled Rolling",*** ISIJ International, **Vol. 32**, No. 3 (1992) pp 258-376

27. Wells M.A., Lloyd D.J., Samarasekera I.V., Brimacombe J.K. and Hawbolt E.B., ***"Modelling Microstructural Changes During Hot Tandem Rolling of AA5XXX Aluminium Alloys: Part 1. Microstructural Evolution",*** Metallurgical and Materials Transactions B, Vol. 29B (June 1998) pp 611-620.

28. Duckham A. and Knutsen R.D., ***"Asymmetric Flow During Plane Strain Compression Testing of Aluminium Alloys",*** Materials Science and Engineering, A256 (1998) pp 220-226.

29. Watts A.B., ***"An Experimental Investigation of the Yielding of Strip Between Smooth Dies",*** Procedures of the Institute of Mechanical Engineers, **Vol.1B**, 10 (1952) pp 448-453

30. Orowan E., ***"The Calculation of Roll Pressure in Hot and Cold Flat Rolling",*** Procedures of the Institute of Mechanical Engineering, **Vol.150,** (1943), pp140-167.

31. Ford H., ***"Research into the Deformation of Metal by Cold Rolling",*** Procedures of the Institute of Mechanical Engineering, **Vol.159** No. 39, (1948), pp115-143.

32. Baxter G.T., Furu T, Whiteman J.A. and Sellars C.M., ***"The Influence of Transient Deformation Condition on Strength, Microstructure and Recrystallisation During Thermomechanical Processing of an Aluminium Alloy Al-1%Mg",*** Material Science Forum, **Vols. 217-222** (1996) pp 459-464.

33. Harris, J.N., ***"Mechanical Working of Metals Theory and Practice",*** International Series on Mat. Science and Tech., **Vol.36**, (1983) pp53-56.

34. Duckham A., **"PhD Thesis"**, University of Cape Town (1998).

35. Beynon, J.H. and Sellars, C.M.,***"Strain Distribution Patterns during Plane Strain Compressions"***, Journal of Testing and Evaluation, JTEV, **Vol.13**, No. 1 (1985), pp 28-320

36. Colas, R. and Sellars, C.M.,"***Strain Distribution and Temperature Increase during Plane Strain Compression Testing***", Journal of Testing and Evaluation, JTEVA, **Vol.15** No.6, (1987) pp342-349.

37. Chen, B. K., Thomas, P. F., and Choi, S. K., ***"Computer Modelling of Microstructure During Hot Flat Rolling of Aluminium",*** Materials Science and Technology, **Vol. 8** (Jan. 1992) pp 72-77.

38. Timothy, S. P., Yui, H. L., Fine, J. M. and Ricks, R. A., ***"Simulation of Single Pass Hot Rolling Deformation of Aluminium Alloy by Plane Strain compression",*** Materials Science Technology, **Vol.7**, March 1991.

39. Gasperini, M., Pinna, C., and Swiatnicki, W., ***"Microstructure Evolution and Strain Localisation During Shear Deformation of an Aluminium Alloy",*** Acta Mat., **Vol.44**, No. 10 (1996) pp 4195-4208,

40. Mirza, M.S., Sellars, C.M., Karhausen, K. and Evans, P., ***"Multipass Rolling of Aluminium Alloys: Finite Element Simulations and Microtructural Evolutions",*** Materials Science and Technology, **Vol. 17** (2001) pp 874 – 87,

41. Boer, C.R., Rebelo, N., Rydstad, H. and Schroder,G., ***"Process Modelling of Metal Forming and Thermomechanical Treatment",*** Materials Research and Engineering, Ed.: Ilshner, B. and Grant, N.J..

42. **"ABAQUS 6.21. Hibbitt"**, Karlsson & Sorensen, United States, 2000.

43. Shi, H., McLaren, A.J., Sellars, C.M., Shahani, R. and Bolingbroke, R., ***"Hot Strain Compression of Aluminium Alloys",*** Journal of Testing and Evaluating, JTEVA, **Vol. 25,** No.1 (1997) pp 61-73.

44. Wittridge, N.J. and Knutsen, R.D., ***"A Microtexture Based Analysis of the Surface Roughening Behaviour of an Aluminium Alloy during Tensile Testing"***, Materials Science and Engineering A269 (1999) pp. 205-216.

45. Aphane, A.K., **"MSc. Thesis"**, University of Cape Town, 2001.

46. **"Struers Metalog Guide"**, Struers Ltd., U.K.

47. Moore, H.D. & Kibbey, D.R. **"Manufacturing: Materials and Processes",** Revised edition, Ohio.

48. Holman, J.P., **"Heat Transfer",** 8th edition, McGraw-Hill International Series.

49. Sanders, R.E Jr., Baumann, S.F. and Stumpf H.C., ***"Non-Heat Treatable Aluminium alloys",*** Proc. Int. Conf. on Aluminium Alloys, Their Physical and Mechanical Properties, Charlotteville, Vol.3, (1986) pp1441.

50. Lenard, J.G. and Pietrzyk, M. ***"Tribology of Hot Forming: Its Effect on Grain Development",*** in ed: Jonas, J.J, Bieler, T.R and Bowman, K.J., "Advances in Hot Deformation Textures and Microstructures", Proc. of Symp., Pittsburgh, October (1993) pp107-119.

9 APPENDICES

9.1 Appendix 1: Input Deck for simulation

```
*HEADING  Rolling simulation
**
*RESTART,WRITE,NUM=3
** BILLET DEF.
**          ----------
*NODE
1, -0.090,     0.00
42, -0.180,    0.00
421, -0.090,   0.013
462, -0.180,   0.013
**
*NGEN,NSET=BOTNDS
1,42,1
*NGEN,NSET=TOPNDS
421,462,1
**
*NFILL,NSET=BILNDS
BOTNDS,TOPNDS,5,84
**
*NSET, NSET=LSIDNDS, GEN
1,421,84
*NSET, NSET=RSIDNDS, GEN
42,462,84
**********************************************
**ELEMENT TYPE & GEN
**          ----------
*ELEMENT,TYPE=CPE4RT
1, 1, 85,86,2
**
*ELGEN,ELSET=BILELS
1, 41,1,1, 5,84,41
*ELSET, ELSET=TOPELS, GEN
165, 205, 1
*ELSET, ELSET=MIDELS, GEN
21, 185, 41
*ELSET, ELSET=LSIDELS, GEN
41,205,41
*ELSET, ELSET=RSIDELS, GEN
1,165,41
**********************************************
** PHYSICAL CONSTANTS
**          ----------
*PHYSICAL CONSTANTS, ABSOLUTE ZERO=-
273.15,
STEFAN BOLTZMANN=5.669E-8
**
** BILLET MAT PROPS
**          ----------
*SOLID SECTION,ELSET=BILELS,
 MATERIAL=AA6061,CONTROL=COMB
 1.30
*SECTION                    CONTROLS,
HOURGLASS=COMBINED, NAME=COMB
**
*MATERIAL, RTOL=1.0, NAME=AA6061
*ELASTIC
6.9E10,.33
**********
*PLASTIC, HARDENING=ISOTROPIC, RATE=0.0
          62.00E06,0
72.00E06,0.1
78.00E06,0.2
85.00E06,0.3
90.00E06,0.4
92.00E06,0.5
93.00E06,0.6
```

```
94.00E06,0.7
95.00E06,0.8
95.50E06,0.9
96.00E06,1.0
**************************
*DENSITY
2.70E3,
*INELASTIC HEAT FRACTION
0.95
*SPECIFIC HEAT
900
*CONDUCTIVITY
180.0
*EXPANSION
2.36.E-5
**
************************************************
**  ROLLER DEFINITION
**          ----------------
*NODE, NSET=ROLLND
10000, 0.06895 ,  0.3580
**
*SURFACE, TYPE=SEGMENTS, NAME=ROLL
START,  0.068950,  0.00800
CIRCL, -.281050,  0.35800 , 0.068950 , 0.3580
**CIRCL .068950,  0. 70800 , 0.068950 , 0.3580
**CIRCL,   .418900,     0.358000  ,  0.068950  ,
0.3580
**CIRCL,   .0689500,    0.008000  ,  0.068950  ,
0.3580
**
*SURFACE, TYPE=ELEMENT, NAME=TOPSURF
TOPELS, S2
LSIDELS, S3
RSIDELS, S1
*RIGID BODY, REF NODE=10000,
ANALYTICAL
SURFACE=ROLL,ISOTHERMAL=YES
**
************************************************
** INITIAL CONDITIONS
**          ----------------
*INITIAL CONDITIONS, TYPE=TEMPERATURE
BILNDS, 288
10000, 150.0
**
************************************************
** STEP 1: COOLING TIME  !!!!!!!!!!
**          ----------------
*STEP
*DYNAMIC   TEMPERATURE-DISPLACEMENT,
EXPLICIT
,1.0
**
*FIXED   MASS   SCALING,   FACTOR=1E8,
ELSET=BILELS
**
**BOUNDARY  CONDITIONS
**          ----------------
*BOUNDARY
BOTNDS,YSYMM
10000,1,2
10000,11,11,150
*BOUNDARY, TYPE=VELOCITY
10000,6,6, 4.2230
**
**HEAT TRANSFER
**          ----------------
*FILM, OP=NEW
 TOPELS, F2, 150.0, 7.5
*RADIATION, OP=NEW
TOPELS, R2, 150.0, 0.8
**
**SURFACE CONTACT
**          ----------------
*CONTACT                  PAIR,MECHANICAL
CONSTRAINT=PENALTY,
INTERACTION=ROLL_TO_AA6061
TOPSURF,ROLL
*SURFACE
INTERACTION,NAME=ROLL_TO_AA6061
*CONTACT  DAMPING,  DEFINITION=CRITICAL
DAMPING FRACTION
0.09
```

```
**
*GAP CONDUCTANCE
15.0E3, 0.0
6.0E3, 0.001
15.0E2,  0.01
*GAP CONDUCTANCE, PRESSURE
30.0E3, 0.0
50.0E3, 1.0E6
80.0E3, 20.0E6
*GAP RADIATION
0.8,  0.8
0.95, 0.0
0.5,  0.0001
0.1,  0.001
0.01,  0.01
*GAP HEAT GENERATION
1.0,  0.5
**
*SURFACE BEHAVIOR, PRESSURE-
OVERCLOSURE=EXPONENTIAL
2.3E-3, 100.0E6, 200.0E9
*FRICTION,TAUMAX=35.8E6
 .3,
**
**REQUIRED OUTPUT
**          ----------------
*OUTPUT,FIELD,NUMBER
INTERVAL=8,TIMEMARKS=YES
*ELEMENT OUTPUT
PEEQ,MISES,PE,TEMP,
*NODE OUTPUT
U,
*OUTPUT,HISTORY,FREQUENCY=100
*ELEMENT OUTPUT, ELSET=MIDELS
SP,PEP,ERV,TEMP,PEEQ
*ENERGY OUTPUT
ALLIE,ALLKE
**
*END STEP
**LOOPING END   !!!!!!!!
**          ----------------
************************************************
**STEP 2: init cond 1st pass !!!!!
**          ----------------------
*STEP
*DYNAMIC    TEMPERATURE-DISPLACEMENT,
EXPLICIT
,0.000001
**
*FIXED    MASS    SCALING,    FACTOR=100.,
ELSET=BILELS
**
**BOUNDARY  CONDITIONS
**          ----------------
*BOUNDARY, TYPE=VELOCITY
BILNDS, 1,1, 1.45734
10000,6,6, 4.2230
**
**HEAT TRANSFER
**          ----------------
*FILM, OP=NEW
  TOPELS, F2, 100.0, 7.5
*RADIATE, OP=NEW
  TOPELS, R2, 100.0, 0.6
**
*OUTPUT,FIELD,NUMBER
INTERVAL=3,TIMEMARKS=YES
*ELEMENT OUTPUT
PEEQ,MISES,PE,TEMP,
*NODE OUTPUT
U,
*OUTPUT,HISTORY,FREQUENCY=20
*NODE OUTPUT, NSET=ROLLND
  RF2,
*ELEMENT OUTPUT, ELSET=MIDELS
SP,PE,ERV,TEMP
*ENERGY OUTPUT
ALLIE,ALLKE
**
*END STEP
** LOOPING END       !!!!!!
**          ----------------
************************************************
**STEP 3: 1ST PASS   !!!!!!!!
```

```
**          ----------
*STEP
*DYNAMIC    TEMPERATURE-DISPLACEMENT,
EXPLICIT
,0.30
**
*FIXED   MASS   SCALING,   FACTOR=100.,
ELSET=BILELS
**
**BOUNDARY CONDITIONS
**      ----------
*BOUNDARY, OP=NEW
BOTNDS,YSYMM
10000,1,2
10000,11,11, 150
**
*BOUNDARY, TYPE=VELOCITY, OP=NEW
10000,6,6, 4.2230
**
*OUTPUT,FIELD,NUMBER
INTERVAL=8,TIMEMARKS=YES
*ELEMENT OUTPUT
PEEQ,MISES,PE,TEMP,
*NODE OUTPUT
U,
*OUTPUT,HISTORY,FREQUENCY=200
*NODE OUTPUT, NSET=ROLLND
 RF2,
*ELEMENT OUTPUT, ELSET=MIDELS
SP,PEP,ERV,TEMP,PEEQ
*ENERGY OUTPUT
ALLIE,ALLKE
**
*END STEP
**OOPING END  !!!!!!
**********************************************
**          STEP 4: DROP ROLLER !!!!!!
**          ----------
*STEP
*DYNAMIC          TEMPERATURE-DISPLACEMENT,
EXPLICIT
,30
**
*FIXED   MASS   SCALING,   FACTOR=1e6.,
ELSET=BILELS
**
**BOUNDARY CONDITIONS
**      ----------
*BOUNDARY, TYPE=VELOCITY
10000,2,2,-0.00004667
*BOUNDARY, TYPE=VELOCITY
BILNDS, 1,1, 0.
**
**
*OUTPUT,FIELD,NUMBER
INTERVAL=5,TIMEMARKS=YES
*ELEMENT OUTPUT
PEEQ,MISES,PE,TEMP,
*NODE OUTPUT
U,
*OUTPUT,HISTORY,FREQUENCY=20
*NODE OUTPUT, NSET=ROLLND
 RF2,
*ELEMENT OUTPUT, ELSET=MIDELS
SP,PE,ERV,TEMP
*ENERGY OUTPUT
ALLIE,ALLKE
**
*END STEP
**LOOPING END  !!!!!
**          ----------
**********************************************
**STEP
**ANNEAL
**END STEP
**********************************************
**STEP 5: init cond 2nd pass  !!!!
**          ----------
*STEP
*DYNAMIC          TEMPERATURE-DISPLACEMENT,
EXPLICIT
,0.00001
**
*FIXED   MASS   SCALING,   FACTOR=100.,
ELSET=BILELS
**
**BOUNDARY CONDITIONS
**      ----------
*BOUNDARY
10000,1,2
**
*BOUNDARY, TYPE=VELOCITY
```

```
BILNDS, 1,1, -1.51156
**
*OUTPUT,FIELD,NUMBER
INTERVAL=3,TIMEMARKS=YES
*ELEMENT OUTPUT
PEEQ,MISES,PE,TEMP,
*NODE OUTPUT
U,
*OUTPUT,HISTORY,FREQUENCY=20
*NODE OUTPUT, NSET=ROLLND
 RF2,
*ELEMENT OUTPUT, ELSET=MIDELS

SP,PE,ERV,TEMP, PEEQ
*ENERGY OUTPUT
ALLIE,ALLKE
**
*END STEP
**LOOPING END  !!!!!!!
**            ----------
**********************************************
**********************************
```

9.2 Appendix 2: Material flow curves

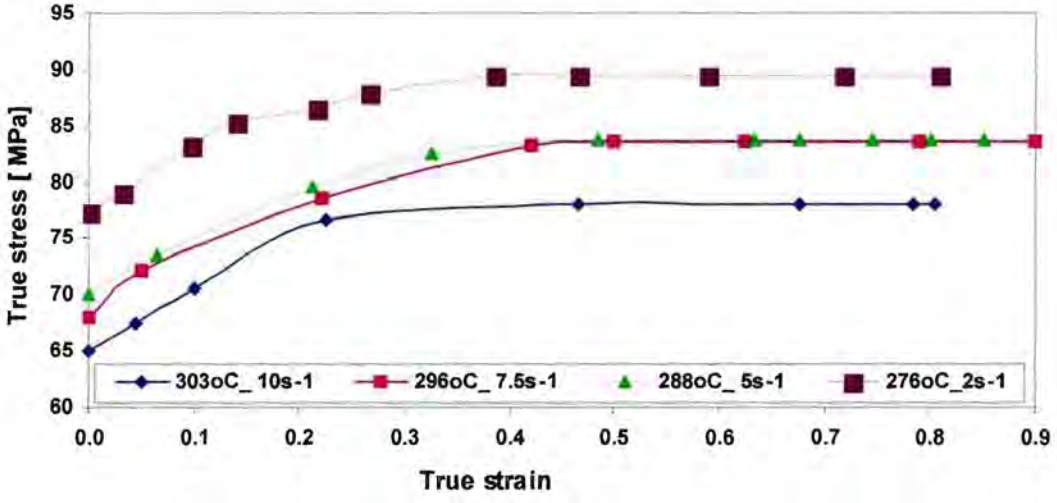

1-pass PSC simulations: varying T and $\dot{\varepsilon}$ to maintain a constant Z (= 7.45E+13).

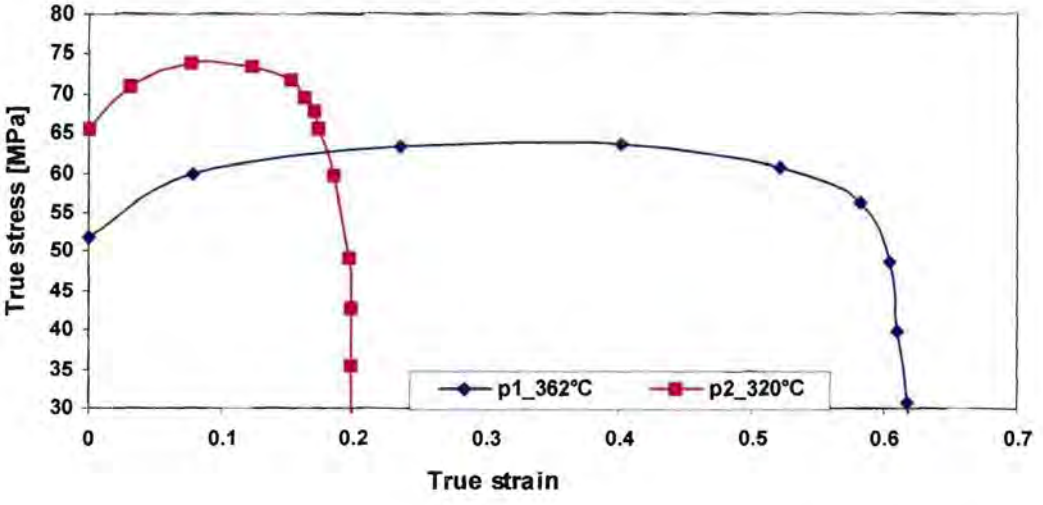

Typical 2-pass PSC simulation: nominal ε_{p1} = 0.6 and ε_{p2} = 0.2 and $\dot{\varepsilon}$ = 10s^{-1}.